ივანე ჯავახიშვილის სახელობის თბილისის სახელმწიფო უნივერსიტეტი

დავით ჭილაძე

ზუსტ და საბუნებისმეტყველო მეცნიერებათა ფაკულტეტი

ფიზიკის მიმართულება

პოლარიზებული გადამუხტვის რეაქციის $dp \to ppn$ შესწავლა ANKE-COSY სპექტრომეტრზე

სადოქტორო დისერტაცია

სადოქტორო პროგრამის ხელმძღვანელი,
თსუ ასოცირებული პროფესორი: სიმონ წერეთელი

სამეცნიერო ხელმძღვანელები:

ფიზ-მათ-მეცნ. დოქტორი, პროფესორი: მიხეილ ნიორაძე

ფიზ-მათ-მეცნ. დოქტორი: ანდრო კაჭარავა

ფიზ-მათ-მეცნ. დოქტორი: ფრანკ რატმანი

თბილისი

2008 წელი

... As our circle of knowledge expands,
so does the circumference of darkness surrounding it.
So the more we know, the more we feel that we don't know.
A. Einstein

Abstract

This thesis describes a study of the analysing powers and differential cross section of the $\overrightarrow{d}\,p \to (pp)n$ reaction for small momentum transfers to a (pp) system with low excitation energy. It is predictied that these observables will allow the direct reconstruction of neutron–proton charge–exchange amplitudes at small scattering angles. This is important for the understanding the NN interaction and therefore for the whole of nuclear physics.

The experiment was performed at the ANKE spectrometer, which is an internal experiment at the COSY storage ring. The polarised deuteron beam of energy 1170 MeV has been used with the hydrogen cluster target. The polarimetry of the beam was performed using the elastic deuteron–carbon scattering at 75.6 MeV and deuteron–proton scattering at 270 MeV. After acceleration to 1170 MeV inside the COSY storage ring, the polarisation of the deuterons were remeasured by studying the analysing powers of a variety of nuclear reactions. The vector (it_{11}) and tensor (t_{20}, t_{22}) analysing powers of the charge–exchange breakup reaction has been extracted. The luminosity determination was performed using two different reactions and this allowed the extraction of the cross–section ($d\sigma/dq$). Finally a good quantitative understanding of all the measured observables is provided by the impulse approximation using known np amplitudes. The proof of principle achieved here for the method suggest that measurements at higher energies will provide useful information in regions where the existing np database is far less reliable.

Contents

Chapter 1

Introduction and motivation

Enormouse progress has been made in subatomic physics during the last century to find the answer to one of man's most ambitious question: "What is the world made of?". A series of important experimental discoveries changed our perceptions about the structure of the matter several times. The current status of our understanding can be displayed in the sequence: molecules $\rightarrow$ atoms $\rightarrow$ nucleis $\rightarrow$ nucleons $\rightarrow$ quarks. The interaction between the fundamental particles (quarks) is described by Quantum Chromo-Dynamics (QCD). The nuclear interaction appears to be a result of interaction between the quarks (i.e. some kind of residual interaction). So the understanding of the nucleon–nucleon (NN) interaction is fundamental to the whole of nuclear physics and hence to the composition of matter as we know it. Apart from its intrinsic importance, it is also a necessary ingredient in the description of meson production and other intermediate energy processes. Thus it is necessary to study it in all its facets in order, together with theory, provide a deep and basic understanding, finally based on the fundamental constituents of matter i.e. quarks and gluons.

The scattering amplitudes for the complete description of the NN interaction can be reconstructed from phase–shift analyses (PSA). The PSA generally need many precise experimental observables as input. The corresponding measurements of these observables require experiments with polarised beam and polarised target, as well as the determination of the polarisation of final–state particles [1]. Many experimental facilities contribute to the database on which such analyses are based and it is incumbent on a laboratory that can make a significant contribution to the communal effort to do so.

1.1 Scientific motivation

The database on proton–proton scattering is enormous thanks to many measurements which have been carried out. The well-known EDDA experiment at COSY has produced the data set of differential cross sections (Fig. 1.1) and the various single and multi–spin observables [2] which have allowed the construction of reliable isospin $I = 1$ phase shifts up to at least 2 GeV [3].

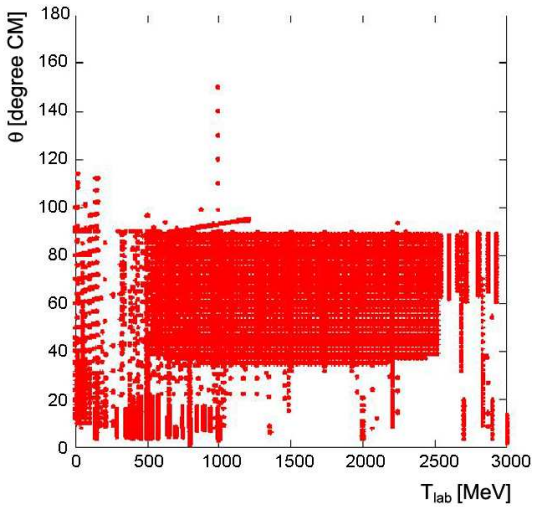

Figure 1.1: Abundance plot of the pp differential cross section $d\sigma/d\Omega$ measurements in the energy *vs* angular domain corresponding to the current status of the SAID date-base. Important to note that in the energy range of $500 < T_p < 2500$ MeV and scattering angle of $30° < \theta_{cm} < 90°$, the plot is dominated by the COSY–EDDA measurements [2]

The situation is far less developed for the isoscalar $I = 0$ case, the corresponding phase shift analysis is only available up to 1.3 GeV and even then there are significant ambiguities at the higher energies [3]. Some of np spin–observables (A_y, A_{yy}) are shown on the Fig 1.2 as an abundance plot, corresponding to the current SAID database [4]. It is seen that above 1 GeV kinetic energy of the proton beam. More good data on neutron-proton scattering are clearly needed, possibly with the aim of directly reconstructing the isosinglet amplitudes at fixed energies. To avoid some of the problems associated with the quality of neutron beams and/or the detection of neutrons, the deuteron is often used successfully as a substitute target or beam.

It was emphasised over 50 years ago that the quasi-free (p, n) or (n, p) reaction on the deuteron can act, in suitable kinematic regions as a spin filter that selects

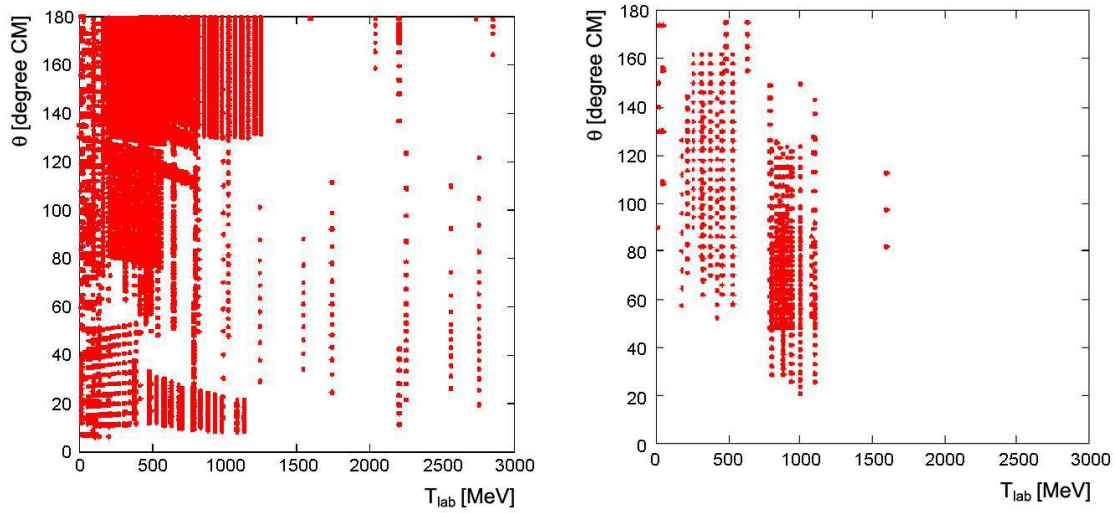

Figure 1.2: Abundance plot some of the np spin–observables: left panel is the analysing power A_y and the right panel is one of the spin–correlation parameter A_{yy} in the energy versus angular domain corresponding to the current status of the SAID date-base.

the spin–dependent contribution to the np elastic cross section [5]. The comparison of this reaction to the free backward elastic scattering on a nucleon target provides the possibility of a direct reconstruction of np backward amplitudes [6]. This work studied in detail the ratio of the forward charge–exchange cross section of a neutron on a deuteron target to that on a hydrogen target.

$$R_{np}(0) = \frac{\mathrm{d}\sigma(nd \to pnn)/\mathrm{d}t}{\mathrm{d}\sigma(np \to pn)/\mathrm{d}t}, \tag{1.1}$$

where t is the four–momentum transfer between the initial neutron and final proton. Due to the Pauli principle, any spin-1 component in the low energy $\{nn\}$ or $\{pp\}$ system is blocked and the system is in the ${}^1S_0$ state. If the data are summed over all excitation energies of the nn system, then the Dean closure sum rule allows one to deduce from R_{np} the fraction of spin–dependence in the pn charge–exchange amplitudes [7].

However, several years ago, it was suggested by Bugg and Wilkin [8] that much more information on the np charge–exchange amplitudes can be extracted by using a polarised deuteron beam or target and studying the charge–symmetric $\overrightarrow{d}\,p \to (pp)n$ reaction. To achieve the full benefit, the excitation energy E_{pp} in the final pp system must be kept low. Experiments from a few hundred MeV up to 2 GeV [9, 10, 11]

have generally borne out the theoretical predictions and have therefore given hope that such experiments might provide valuable data on the amplitudes in the small momentum transfer region.

The ANKE collaboration is embarking on a systematic programme to significantly improve our knowledge of np elastic scattering by measuring cross-sections, analysing powers, and spin-correlation coefficients in both forward and backward directions of the $\vec{d}\vec{p} \to n\{pp\}$ reaction up to the maximum energy of the COSY accelerator of 1.15 GeV per nucleon [12]. Higher energies per nucleon will be achieved through the use of proton beam and a deuterium target. The aim of this thesis is to provide the check of the methodology in a region where the neutron–proton amplitudes are reasonably well known. This proof-of-principle of the approach will be demonstrated in the following sections of this thesis.

1.2 np-Amplitudes and charge-exchange on the deuteron

In single scattering (impulse) approximation [8] the deuteron charge exchange reaction $\overrightarrow{d}\,p \to (pp)n$ can be considered as $np \to pn$ reaction with a spectator proton. Initially the np are in bound state in deuteron and the final pp pair are subject of the final state interaction, as illustrated diagrammatically in Fig. 1.3. If $\vec{k}$ relative momentum in the pp system is small and hence $E_{pp} = \vec{k}^2/m$ is small then the final pp pair is in $^1S_0$ state. This reaction acts as spin-isospin filter from ($^3S_1$, $^3D_1$) deuteron to the $^1S_0$ (pp). Furthermore if the relative momentum $\vec{q} = \vec{k}_f - \vec{k}_i$ is small the other final states are very weakly excited. Under such condition the resulting matrix element is proportional to that for $np \to pn$ times form factor which depends on deuteron and pp wave functions and also $\vec{q}$, the momentum transfer. There is a strong interplay between the $np \to pn$ amplitudes and the polarisation of the deuteron which leads to a strong tensor analysing power signal. It should be noticed that the analysing powers have opposite signs for spin-singlet and spin-triplet pp final states [8]. As a consequence it leads to the dilution of the effect if the higher waves are excited. We present the formalism for pure $S-$wave state but for the detailed comparison of the data with theory a much more thorough numerical evaluation is required [13].

The charge–exchange amplitude of the elementary $np \to pn$ scattering may be

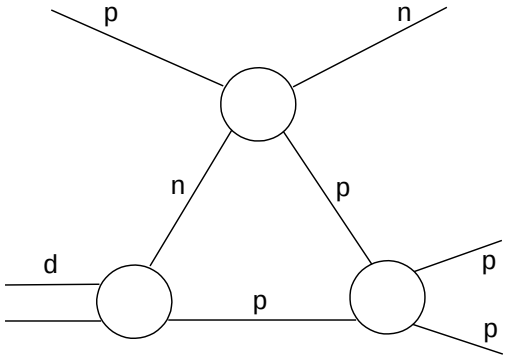

Figure 1.3: Impulse approximation diagram for nucleon charge exchange on the deuteron

written in terms of five scalar amplitudes in the cm system as

$$\begin{aligned} f_{np} &= \alpha(q) + i\gamma(q)(\vec{\sigma}_1 + \vec{\sigma}_2)\cdot\vec{n} + \beta(q)(\vec{\sigma}_1\cdot\vec{n})(\vec{\sigma}_2\cdot\vec{n}) \\ &\quad +\delta(q)(\vec{\sigma}_1\cdot\vec{m})(\vec{\sigma}_2\cdot\vec{m}) + \varepsilon(q)(\vec{\sigma}_1\cdot\vec{l})(\vec{\sigma}_2\cdot\vec{l}), \end{aligned} \tag{1.2}$$

where $\vec{\sigma}_1$ is the Pauli matrix between the initial neutron and final proton, and the reverse for $\vec{\sigma}_2$. As stressed in Ref. [6], α is the spin–independent amplitude between the initial neutron and final proton, γ is a spin–orbit contribution, and β, δ, and ε are the spin–spin terms. The one–pion–exchange pole is contained purely in the δ amplitude and this gives rise to its very rapid variation with momentum transfer, which influences very strongly the deuteron charge–exchange observables.

The orthogonal unit vectors are defined in terms of the initial neutron ($\vec{k_i}$) and final proton ($\vec{k_f}$) momenta;

$$\vec{n} = \frac{\vec{k}\times\vec{k'}}{|\vec{k}\times\vec{k'}|}, \quad \vec{m} = \frac{\vec{k'}-\vec{k}}{|\vec{k'}-\vec{k}|}, \quad \vec{l} = \frac{\vec{k'}+\vec{k}}{|\vec{k'}+\vec{k}|}\,. \tag{1.3}$$

The amplitudes are normalised such that the elementary $np \to pn$ differential cross section has the form

$$\left(\frac{\mathrm{d}\sigma}{\mathrm{d}t}\right)_{np\to pn} = |\alpha(q)|^2 + |\beta(q)|^2 + 2|\gamma(q)|^2 + |\delta(q)|^2 + |\varepsilon(q)|^2\,. \tag{1.4}$$

In impulse approximation the deuteron charge–exchange amplitude to the $^1S_0$ state depends only upon the spin–dependent parts of f_{np} [8]. The form factor de-

scribing the transition from a deuteron to a $^1S_0$–state of the final pp pair contains two terms

$$\begin{aligned} S^+(k,\frac{1}{2}q) &= F_S(k,\frac{1}{2}q) + \sqrt{2}F_D(k,\frac{1}{2}q)\,, \\ S^-(k,\frac{1}{2}q) &= F_S(k,\frac{1}{2}q) - F_D(k,\frac{1}{2}q)/\sqrt{2}\,. \end{aligned} \tag{1.5}$$

Here $\vec{q}$ is the three–momentum transfer between the proton and neutron which, for small E_{pp}, is related to the four–momentum transfer by $t = -\vec{q}^2$.

The S^+ and S^- denote the longitudinal ($\lambda = 0$) and transverse ($\lambda = \pm 1$) form factors, where λ is the spin–projection of the deuteron. The matrix elements F_S and F_D can be expressed in terms of the S– and D–state components of the deuteron wave function $u(r)$ and $w(r)$ and the pp ($^1S_0$)–scattering wave function $\psi_k^{(-)}(r)$ as

$$F_S(k,\frac{1}{2}q) = \langle \psi_k^{(-)} | j_0(\frac{1}{2}qr) | u \rangle\,, \tag{1.6}$$

$$F_D(k,\frac{1}{2}q) = \langle \psi_k^{(-)} | j_2(\frac{1}{2}qr) | w \rangle. \tag{1.7}$$

Here $\vec{k}$ is the pp relative momentum, corresponding to an excitation energy $E_{pp} = \vec{k}^2/m$, where m is the proton mass. We denote the ratio of the transition form factors by

$$\mathcal{R} = S^+(k,\frac{1}{2}q) \Big/ S^-(k,\frac{1}{2}q) \tag{1.8}$$

and the combination of modulus–squares of amplitudes by

$$I = |\beta(q)|^2 + |\gamma(q)|^2 + |\varepsilon(q)|^2 + |\delta(q)|^2|\mathcal{R}|^2. \tag{1.9}$$

Impulse approximation applied to $dp \to \{pp\}_{^1S_0} n$ then leads to the following predictions for the differential cross section and deuteron spherical analysing powers [8, 13]:

$$\begin{aligned} \frac{\mathrm{d}^4\sigma}{\mathrm{d}t\,\mathrm{d}^3k} &= I \left[S^-(k,\frac{1}{2}q) \right]^2 \Big/ 3, \\ I\,it_{11} &= 0\,, \\ I\,t_{20} &= \left[|\beta(q)|^2 + |\delta(q)|^2|\mathcal{R}|^2 - 2|\varepsilon(q)|^2 + |\gamma(q)|^2 \right] / \sqrt{2}\,, \\ I\,t_{22} &= \sqrt{3} \left[|\beta(q)|^2 - |\delta(q)|^2|\mathcal{R}|^2 + |\gamma(q)|^2 \right] / 2\,. \end{aligned} \tag{1.10}$$

In this $^1S_0$ limit, a measurement of the differential cross section, t_{20}, and t_{22} would

allow one to extract values of $|\beta(q)|^2 + |\gamma(q)|^2$, $|\delta(q)|^2$, and $|\varepsilon(q)|^2$ for small values of the momentum transfer $\vec{q}$ between the initial proton and final neutron. However, even if a sharp cut of 1 MeV is placed upon E_{pp}, there still remain small contributions from proton–proton P–waves that dilute the analysing power signal. Such effects must be included in any analysis aimed at providing quantitative information on the neutron–proton amplitudes [13].

One way of reducing the dilution of the tensor analysing powers by the P–waves is by imposing a cut on the angle θ_{qk} between the momentum transfer $\vec{q}$ and the relative momentum $\vec{k}$ between the two protons. When these two vectors are perpendicular, impulse approximation does not allow the excitation of odd partial waves in the pp system [8] and this is in agreement with available experimental data [11].

In terms of the charge–exchange amplitudes, the Dean sum rule [7] for the ratio of the forward $nd \to pnn$ to $np \to pn$ cross sections of Eq. (1.1) becomes

To avoid the explicit introduction of the dynamics of the low energy NN system, Dean [7] derived a sum rule for the ratio R_{np} (Eq. 1.1), as a function of the momentum transfer q. In collinear dynamics, where there is no dependence on the deuteron structure it simplifies to

$$R_{np}(0) = \frac{2}{3}\left[\frac{2|\beta(0)|^2 + |\varepsilon(0)|^2}{|\alpha(0)|^2 + 2|\beta(0)|^2 + |\varepsilon(0)|^2}\right] \tag{1.11}$$

The sum rule of Eq. (1.11) is very effective at medium and high energies because it converges so quickly. The same result should, of course, hold for $dp \to (pp)n$, which is the reaction studied at ANKE.

The work carried out in this thesis shows that the method suggested above works and will allow to obtain the useful information for higher energies where the existing np database is poorly known.

Chapter 2

Experimental equipment: COSY and ANKE

The experiment have been performed at the magnetic spectrometer ANKE at the COoler SYnchrotron COSY. In order to study the Charge–Exchange deuteron breakup reaction, the forward detection system of the ANKE spectrometer and the Silicon Tracking Telescope (STT) were used. The forward system allows the detection of charged particles emitted at small forward angles and high momenta. The STT system was used to measure very slow particles emerging from the thin target and, in particular, allowed the identification and tracking of the recoil protons. In this chapter a technical overview of the accelerator and the detector systems is given.

2.1 Accelerator and storage ring COSY

The accelerator and storage ring **COSY** (**Co**oler **SY**nchrotron) [14] at the *Forschungszentrum Jülich* can provide high quality, high precision polarised and unpolarised, proton (p) and deuteron (d) beams. H^- and D^- ions are pre–accelerated in the cyclotron JULIC and injected into the storage ring via a charge–exchanging stripper carbon foil. The layout of COSY is shown in Fig. 2.1. The total circumference of the storage ring is 184 m. This machine covers the momentum range from 295 MeV/c up to 3.65 GeV/c, corresponding to an energy range between 45 MeV and 2.83 GeV for protons, and from 23 MeV to 2.23 GeV for deuterons. COSY provides ion beams with a momentum resolution of $\Delta p/p = 10^{-3} - 10^{-5}$ and delivers up to $6{\times}10^{10}$ pro-

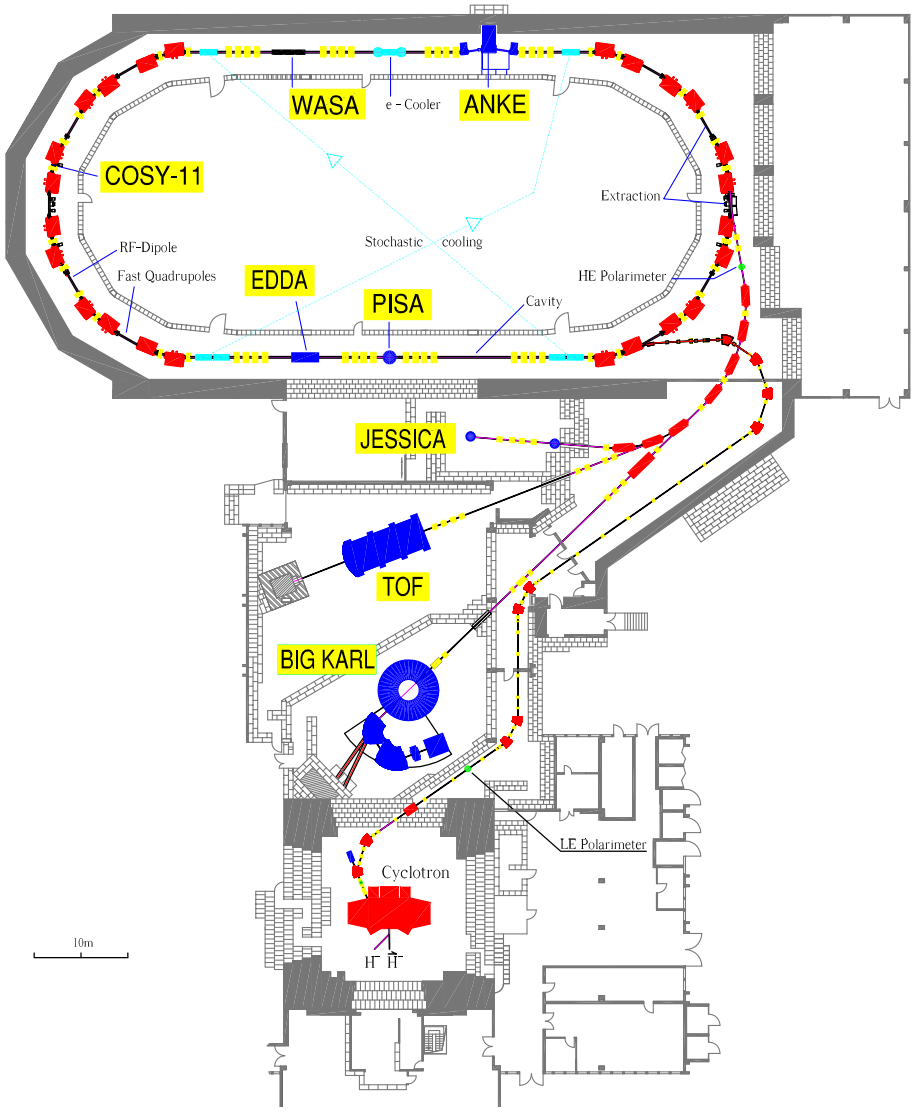

Figure 2.1: The COoler SYnchrotron COSY at the Forschungszentrum Jülich.

tons/deuterons in the ring (space charge limit is $\approx 2\times10^{11}$ p). Electron cooling is applied up to 645 MeV/c. Also a stochastically cooled beam [15, 16] can be provided in order to achieve the highest phase space density and to compensate beam deterioration due to beam-target interactions. This can be applied in the momentum range from 1.5 to 3.3 GeV/c. COSY beams are being delivered to internal (ANKE, WASA, COSY–11, EDDA) and external experiments (TOF, BIG KARL), but the latter are not of importance for the current discussion.

2.1.1 Polarised ion source

The polarised colliding–beams source at COSY [17, 18, 19] comprises three major groups of components, the pulsed atomic beam source, the cesium beam source, and the charge–exchange and extraction region. The set–up is shown schematically in Fig. 2.2. The atomic beam source produces an intense pulsed polarised atomic

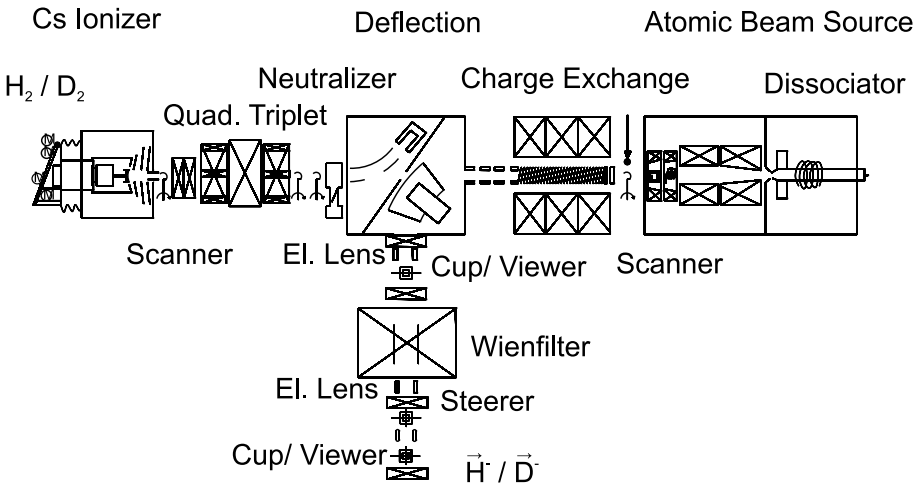

Figure 2.2: Set–up of the polarised ion source at COSY.

hydrogen or deuterium beam. The gas molecules are dissociated in an inductively coupled rf discharge and a high degree of dissociation is maintained by having a special admixture of small amounts of nitrogen and oxygen that reduce surface and volume recombination. The current output of the source depends sensitively on the relative fluxes of the gases and on their timing with respect to the dissociator radio frequency. The atoms are cooled to about 30 K by passing through an aluminum nozzle of 20 mm length and 3 mm diameter and the resulting beam is focused by an optimised set of permanent hexapoles into the charge–exchange region. By cooling the supersonic atomic beam, the acceptance of the hexapole system and the dwell time in the charge–exchange region are increased, though scattering in the vicinity of the nozzle reduces partially these beneficial effects. A peak intensity of 7.5×10^{16} atoms/s has been measured within a diameter of 10 mm at the exit of the hexapole chamber. The atomic $\vec{H}^\circ$ beam with high nuclear polarisation collides with the fast neutral Cs beam inside the charge–exchange region and an electron is transferred through the $\vec{H}^\circ + Cs^\circ \rightarrow \vec{H}^- + Cs^+$ reaction. The $\vec{H}^-$ ions are extracted from this region by electric fields before being deflected magnetically through 90°.

Subsequently they pass a Wien filter that provides the proper spin alignment for injection into the cyclotron JULIC, which is the preaccelerator for COSY.

The fast neutral cesium beam is produced in a two–step process. Cesium vapour is thermally ionised on a hot porous tungsten surface at a beam potential around 45 kV and the beam is then focused by a quadrupole triplet to the charge–exchange region. The space–charge compensation of the intense beam is improved by feeding 10^{-3} mbarℓs^{-1} argon to the beam tube following the extraction. Cesium sputtering and contamination generally impedes long–term reliability so that pulsed operation of the cesium ioniser has been included in the source [20]. The cesium pulses reach peak intensities of over 10 mA with a width of about 10 ms. For routine operation, cesium pulses with a 5 mA flat shape of 20 ms width and a repetition rate of 0.5 Hz are used [19], matched to the COSY injection scheme. A neutraliser is placed between the quadrupoles and the cesium deflector. This consists of a cesium oven, a cell filled with cesium vapour, and a magnetically driven flapper valve between the oven and the cell. The remaining Cs^+ beam is deflected in front of the solenoid to the cesium cup. Routinely, a neutraliser efficiency of over 90% is achieved.

The highly selective charge–exchange ionization produces only little unpolarised background that would reduce the nuclear beam polarisation. In the charge–exchange region, various beam properties can be adjusted. Transverse emittance can be traded for polarisation by varying the solenoid's magnetic field. The field strength during normal operation is 1.8 kG. The magnitude of the electrical drift field inside the solenoid can be tuned to optimise the energy spread of the beam. The electric field gradient amounts to 0.5–1.0 V/m. A monotonic gradient, in combination with a double buncher system in the injection beam line to the cyclotron, leads to an improved bunching factor of about four, compared to a factor of two for unpolarised beams.

Without modification of the system, the colliding–beams ion source can provide negatively–charged polarised hydrogen and deuterium beams of comparable intensities. To prepare polarised deuterons with the desired combinations of vector and tensor polarisation, the atomic beam part of the source is equipped with new radiofrequency transitions (RFTs). These transition units are operated at the magnetic fields and radiofrequencies that allow exchange of occupation numbers of the different hyperfine states in deuterium [21]. A set of three installed devices, RFT_1 to RFT_3, allows a large number of combinations to be delivered to experiments, as described in the following section.

2.1.2 Acceleration of polarised beams at COSY

The polarised H^- or D^- ion beam delivered by the source, is pre-accelerated in the cyclotron JULIC and injected by charge exchange into the COSY ring. The acceleration of vertically polarised protons and deuterons at COSY is discussed in detail, for example, in [22].

For an ideal planar closed–loop accelerator with a vertical guide field, the particle spin vector precesses around the vertical axis. In this way the vertical beam polarisation is preserved. The spin motion in an external electromagnetic field is governed by the Thomas–BMT equation, leading to a spin tune $\nu_{sp} = \gamma G$, which describes the number of spin precessions of the central beam per revolution in the ring. G is the anomalous magnetic moment of the particle ($G = 1.7928$ for protons, -0.1423 for deuterons), and $\gamma = E/m$ is the Lorentz factor. During the acceleration of a vertically polarised beam, depolarising resonances are crossed if the precession frequency of the spin γG is equal to the frequency of the encountered spin–perturbing magnetic fields. In a strong–focusing synchrotron like COSY, two different types of strong depolarising resonances are excited, namely imperfection resonances caused by magnetic field errors and misalignments of the magnets, and intrinsic resonances excited by horizontal fields due to the vertical focusing. For deuterons the spin tune is about 25 times lower than for protons at the same energy. Depolarising resonances for deuterons are therefore 25 times further apart compared to those for protons. Depolarising resonances for deuterons are also about 13 times weaker than for protons at low energies and 25 times weaker for high energies.

In the momentum range of COSY, five imperfection resonances have to be crossed for protons. The existing correction dipoles of COSY are utilised to overcome all imperfection resonances by exciting adiabatic spin flips without polarisation losses. The number of intrinsic resonances depends on the superperiodicity of the lattice. The magnetic structure of COSY allows one to choose a superperiodicity of $P = 2$ or 6. A tune-jump system consisting of two fast quadrupoles has been developed especially to handle intrinsic resonances at COSY. The depolarisation resonances for the deuterons are out of the COSY momentum range. Hence there shouldn't be any depolarisation of deuterons during acceleration up to highest COSY energy, which is confirmed also by experimental measurements.

The imperfection resonances for protons in the momentum range of COSY are listed in Table 2.1. They are crossed during acceleration, if the number of spin

precessions per revolution of the particles in the ring is an integer ($\gamma G = k, k$ is integer). The resonance strength depends on the vertical closed orbit deviation.

γG	T_p GeV	p GeV/c	y_{co}^{rms} mm	ϵ_r 10^{-3}	P_f/P_i
2	0.1084	0.4638	2.3	0.95	-1.00
3	0.6318	1.2587	1.8	0.61	-0.88
4	1.1551	1.8712	1.6	0.96	-1.00
5	1.6785	2.4426	1.6	0.90	-1.00
6	2.2018	2.9964	1.4	0.46	-0.58

Table 2.1: Resonance strength ϵ_r and the ratio of preserved polarisation P_f/P_i at imperfection resonances for a typical vertical orbit deviation y_{co}^{rms}, without considering synchrotron oscillation.

A spin flip occurs at all resonances if synchrotron oscillations are not considered. However, the influence of synchrotron oscillation during resonance crossing cannot be neglected. After the first imperfection resonance, the calculated polarisation with a momentum spread of $\Delta p/p = 1 \times 10^{-3}$ and a synchrotron frequency of $f_{syn} =$ Hz is about $P_f/P_i \approx -0.85$. The resonance strength of the first imperfection resonance has to be enhanced to $\epsilon_r = 1.6 \times 10^{-3}$ to excite spin flips with polarisation losses of less than 1%. At the other imperfection resonances the effect of synchrotron oscillation is smaller, due to the lower momentum spread at higher energies. Vertical correction dipoles or a partial Siberian snake could be used to preserve polarisation at imperfection resonances by exciting adiabatic spin flips. Simulations indicate that an excitation of the vertical orbit with existing correction dipoles by 1 mrad is sufficient to adiabatically flip the spin at all imperfection resonances. In addition, the solenoids of the electron-cooler system inside COSY are available for use as a partial snake. They are able to rotate the spin around the longitudinal axis by about 8° at the maximum momentum of COSY. A rotation angle of less than 1° of the spin around the longitudinal axis already leads to a spin flip without polarisation losses at all five imperfection resonances. The number of intrinsic resonances depends on the superperiodicity P of the lattice, which is given by the number of identical periods in the accelerator. The COSY ring consists of two 180° arc sections connected by straight sections. The straight sections can be tuned as telescopes with 1:1 imaging, giving a 2π betatron phase advance. In this case the straight sections are optically transparent and the arcs contribute to the strength of intrinsic resonances. One then

obtains for the resonance condition $\gamma G = k \times P \pm (Q_y - 2)$, where k is an integer and Q_y is the vertical betatron tune. The magnetic structure in the arcs allows adjustment of the superperiodicity to $P = 2$ or 6. The corresponding intrinsic resonances in the momentum range of COSY are listed in Table 2.2.

P	γG	E_{kin} MeV	p MeV/c	ϵ_r 10^{-3}
2	$6 - Q_y$	312.4	826.9	0.26
2	$0 + Q_y$	950.7	1639.3	0.21
2,6	$8 - Q_y$	1358.8	2096.5	1.57
2	$2 + Q_y$	1997.1	2781.2	0.53
2	$10 - Q_y$	2405.2	3208.9	0.25

Table 2.2: Resonance strength ϵ_r of intrinsic resonances for a normalized emittance of 1π mm mrad and vertical betatron tune of $Q_y = 3.61$ for different superperiodicities P.

2.1.3 Polarised deuteron beam

The first injection and acceleration of vertically polarised deuterons for this experiment was performed in February 2003. No first-order depolarising resonance is crossed in the momentum range of COSY at an standard transversal betatron tune.

The actual experiment used the polarised deuteron beam provided by the COSY ion source. After selection of electronic states $m_j = +\frac{1}{2}$, the deuteron nuclei are still not polarised since the beam contains equal population of the three deuterium magnetic substates. Usually radio-frequency transitions (RFT) are applied to induce exchange between magnetic sub–levels $|m_j, m_d\rangle$ in order to produce nuclear polarisation. In the November 2003 run, the following set of transitions was used for the preparation of the polarised COSY deuteron beam:

RFT1 high-field single transition 361 MHz:

$$|-1/2, -1\rangle \Longleftrightarrow |-1/2, 0\rangle$$

RFT2 middle-field single transition 328 MHz:

$$|1/2, 0\rangle \Longleftrightarrow |1/2, 1\rangle$$

RFT3 weak-field triple transition 5.8 MHz:

$$\begin{aligned} |3/2,1\rangle &\quad\Longleftrightarrow\quad |-3/2,-1\rangle \\ |1/2,0\rangle &\quad\Longleftrightarrow\quad |-1/2,-1\rangle \\ |-1/2,0\rangle &\quad\Longleftrightarrow\quad |1/2,1\rangle \end{aligned}$$

The final scheme consists of eight different polarisation states, including one unpolarised mixture and seven combinations of vector and tensor polarisations, as shown in Table 2.3.

Mode	Patt.	P_z^{Ideal}	P_{zz}^{Ideal}	I_0^{Ideal}	6pole$_1$	RFT1	6pole$_2$	RFT2	RFT3	m_l
0	000	0	0	1	123	123	123	123	123	+1,0,–1
1	001	$-\frac{2}{3}$	0	1	123	123	123	123	432	–1,–1,0
2	010	$+\frac{1}{3}$	+1	1	123	123	123	163	163	+1,+1,–1
3	011	$-\frac{1}{3}$	–1	1	123	123	123	163	452	–1,0,0
4	100	$+\frac{1}{2}$	$-\frac{1}{2}$	$\frac{2}{3}$	123	125	12	12	12	+1,0
5	101	–1	+1	$\frac{2}{3}$	123	125	12	12	43	–1,–1
6	110	+1	+1	$\frac{2}{3}$	123	125	12	16	16	+1,+1
7	111	$-\frac{1}{2}$	$-\frac{1}{2}$	$\frac{2}{3}$	123	125	12	16	45	–1,0

Table 2.3: The table lists the eight configurations of the polarised deuteron ion source, showing the ideal values of the vector and tensor polarisations and the relative beam intensities obtained by operating the three radiofrequency transitions (RFTs).

For each injection into COSY, the polarised ion source was switched to a different polarisation state. The duration of a COSY cycle was sufficiently long (200 sec) to ensure stable conditions for the injection of the next state. After the seventh state, the source was reset to the zeroth mode and the pattern repeated for the next injection. The ANKE data acquisition system received status bits from the source, latched during injection, that ensured the correct identification of the polarisation states during the experiment. Because of their small magnetic moment, deuterons encounter no depolarising resonances in the energy range of COSY and are therefore unlikely to be depolarised. This was recently tested for a vector polarised beam, at least qualitatively, during the SPIN@COSY experiment [12]. It should be noted, that the present ANKE experiment is the first one that provides at the same time a measurement of both vector and tensor polarisations of the deuteron beam stored in COSY.

2.2 ANKE spectrometer and detection system

The experiment was performed at the ANKE spectrometer [23] ("Apparatus for studies of Nucleon and Kaon Ejectiles") installed at the internal beam of COSY. In Fig. 2.3 the ANKE spectrometer is shown. The main components of the spectrom-

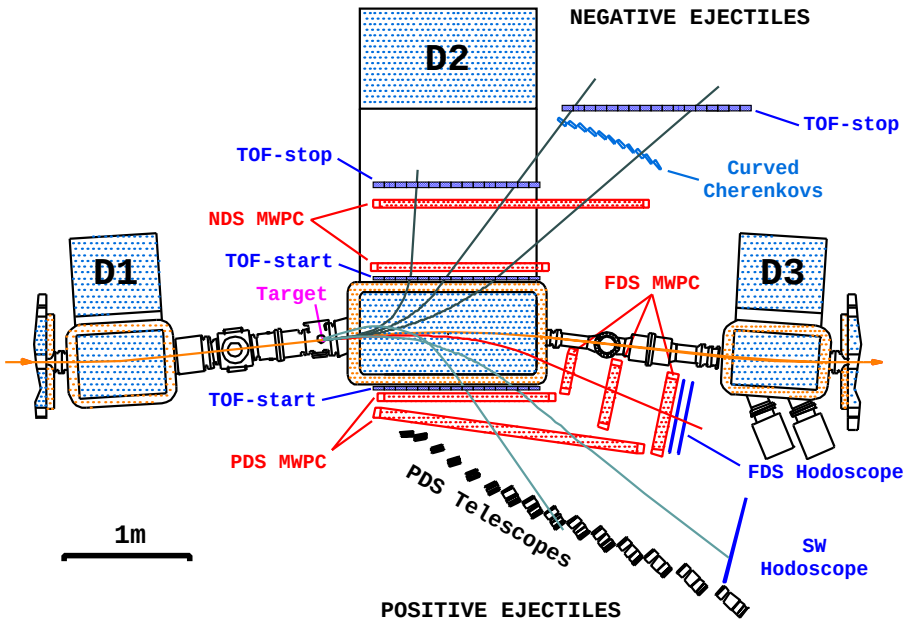

Figure 2.3: Schematic drawing of ANKE Spectrometer

eter are: a magnetic system, an internal target and four detection systems: positive and negative side detectors, forward and backward detectors. The ANKE magnetic system consists of a dipole magnet D1 which deflects the circulating COSY beam by an angle α, a large spectrometer dipole magnet D2 (beam deflection -2α), and a third dipole magnet D3, identical to D1, to deflect the beam by α back to the nominal orbit. The deflection angle of the beam can be adjusted to optimise the magnetic field up to 1.56 T independent of the COSY beam momentum.

There are three types of targets available at ANKE: (*i*) a strip target (carbon, polyethylene or any other solid material); (*ii*) a cluster beam target [24], producing a beam of hydrogen or deuterium clusters that cross the COSY beam; and (*iii*) a polarised storage-cell gas target [25], fed by an atomic beam source (ABS) for polarisation measurements. The momentum acceptance of the positive and negative side detectors is in the range of about 0.3 to 0.8 GeV/c. The forward detector, allowing one to detect positively charged particles in momentum range 0.3–3.7 GeV/c, is

used in a number of experiments at ANKE, e.g. the a_0 production study [26], the ω, η production on effective neutron target [27, 28], the deuteron breakup study [29], charge exchange breakup [30], etc.

2.2.1 Forward Detector system

In Fig. 2.4 those parts of the spectrometer are shown that are relevant for the present experiment. The forward detector (FD) is located between the spectrometer dipole

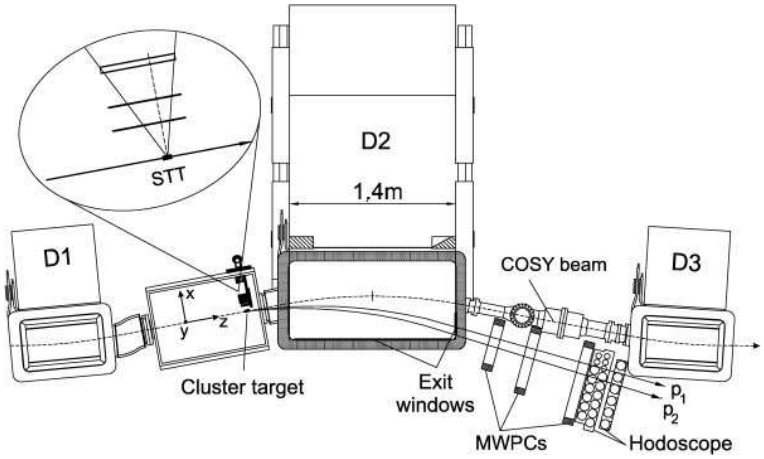

Figure 2.4: Schematic drawing of the part of ANKE used in the $\vec{d}p \to (pp)+n$ experiment

D2 and the dipole D3, though the available space is rather limited there. The gap between the dipoles is 1.6 m in length and the distance between the accelerator beam tube and the ANKE side detector is about 0.7 m. Such a location results in severe requirements on the tracking system. Due to closeness to the beam pipe, it must be able to operate at rather high counting rates ($> 10^5 \mathrm{s}^{-1}$). In addition, because of the short distance between the MWPCs, one has to achieve high spatial resolution (better than 1 mm). Such spatial resolution leads to a momentum resolution of about 1%, which allows one to distinguish proton pairs with small excitation energy $E_{pp} < 3$ MeV. Particles emitted at small angles and high momenta pass the detector region close to the beam pipe, which means that the width of the chamber frame must be minimised on the side of the beam pipe.

The FD system comprises three MWPCs in total. Each of them is composed of one X and one Y module. Every module contains a wire and a strip plane. In what follows, the planes located in an $X(Y)$ module will be referred to as the $X(Y)$.

Wires are oriented vertically in the X wire planes, and horizontally in the Y planes. The strips are inclined by 18° with respect to the vertical axis in the X planes, and at $-18°$ in the Y planes. The MWPCs are mounted on a common support frame with the forward hodoscope.

The chambers produce signals 6 ns long (FWHM) for the wire planes and 30 ns long for the strip ones. The time jitter of the signals is small, being around 8 ns for the wire pulses. This allows effective operation with short strobe signals. At the set-up, the time resolution of the tracking system is limited by the read-out electronics [31], which need strobes more than 50 ns wide (while the chambers themselves could work with much shorter strobe pulses). The average number of wires fired by a crossing particle (cluster width) is close to unity, which leads to a high precision of coordinate measurements.

The hodoscope consists of two layers, containing 8 and 9 vertically oriented scintillators (4 to 8 cm width, 1.5 to 2 cm thickness). The timing and amplitude signals are read out via photomultipliers placed on both ends of each scintillator. They provide a trigger signal, an energy loss measurement, and allows for the determination of the differences in arrival times for particle pairs hitting different counters. Off-line processing of the amplitude data permitted the measurement of the energy-loss with 10% accuracy, and of the time-of-flight difference of events with two registered particles with a precision of 0.5 ns (rms). The third layer was implemented mainly to identify ^{3}He.

The angular acceptance of the FD is about 12° in the horizontal plane and about 3.5° in the vertical plane.

2.2.2 Silicon Tracking Telescope

For the identification and tracking of slow recoil protons, a Silicon Tracking Telescope (STT) has been developed [32] that can be operated inside the ultra high vacuum of the accelerator. The basic detection concept of the STT combines proton identification with tracking over a wide range in energy. The tracking is accomplished by three layers of double–sided micro–structured silicon strip detectors that can be placed close to the target inside the vacuum chamber (see Fig. 2.4). The set–up of the STT and a photo is shown in Fig. 2.5.

Measuring the energy loss in the individual layers allows identification of stopped

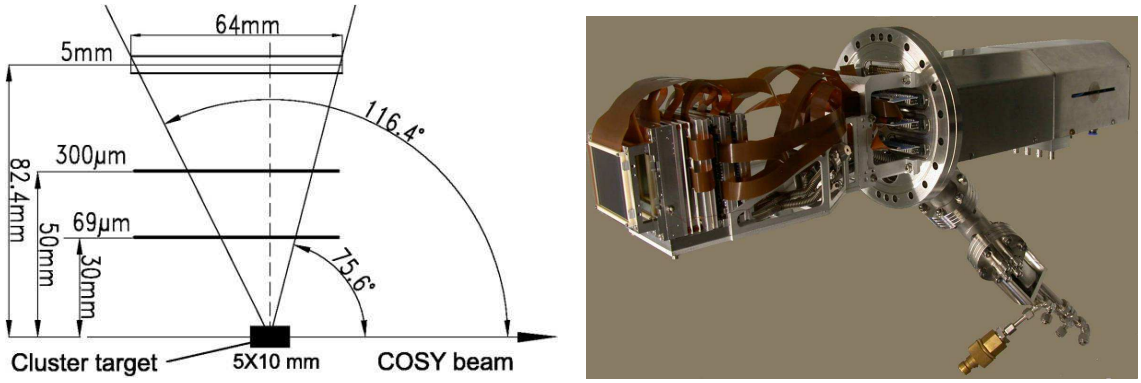

Figure 2.5: Left: Top view of the Silicon Tracking Telescope (STT), consisting of three layers of different thickness. The approximate extension of the cluster target beam in the x–z plane is indicated, along with the approximate polar angles covered. **Right:** Photo of one of the STT module including cooling and readout electronics

particles by the ΔE/E method. A proton is registered when it passes through the first layer and is stopped in the second layer, so that the minimum energy of a proton that can be tracked is determined by the thickness of the innermost layer. The maximum energy of tracked protons is given by the range within the telescope and therefore by the total thickness of all detection layers. Therefore, the primary design goal in the development of the STT was to combine the thinnest possible innermost with the thickest available outermost layer of the silicon detector.

A first generation STT [33] was already equipped with three detection layers: a non–structured 60 μm thick layer, a single–sided structured 300 μm, and a 5100 μm thick detector. Although serving mainly as a prototype system with limited size and poor tracking capabilities, it allowed us to study the reactions quasi-free $pn \to d\pi^\circ$ [33] and, $pn \to d\omega$ [34]. In addition it was also used as a polarimeter [35].

The new STT employs the well–established thicknesses of the first generation system, but overcomes the limited tracking capabilities by using double–sided micro–structured detectors. The angular coverage in the forward hemisphere was small, because the position of the STT with respect to the target was optimised to detect slow recoil protons in the backward hemisphere. Nevertheless, protons emitted at angles from about 75° to 80° were unambiguously identified in the STT in coincidence with elastically scattered deuterons in the FD.

The new STT facilitates ΔE/E proton identification from 2.5 up to 40 MeV with an energy resolution of 150–250 keV (FWHM). Particle tracking is possible over a wide range of energies with an angular resolution varying from 1° to 6° (FWHM).

The resolution is limited by angular straggling within the detectors and therefore depends on particle type, energy, and track inclination. The geometrical limit is defined by the strip pitch (ranging from 400 to 666 μm) and the distances between the detectors. The STT has self–triggering capabilities. It identifies a particle passage within 100 ns and provides the possibility for fast timing coincidences with other detector components of the ANKE spectrometer, whereby accidental coincidences can be suppressed significantly. The high rate capabilities of the STT will be especially important for the upcoming polarisation experiments [12], because then two or more STTs have to be placed in the forward hemisphere. The recent development of very thick (> 10 mm) double–sided micro–structured Si(Li) detectors will allow us to extend further the accessible energy range of the STT [36].

2.3 Data-taking conditions

During this first measurement we aimed to take data with a vertically polarised deuteron beam and an unpolarised target. The polarised deuterons stored in the COSY ring ($\approx 3\times10^9$ deuterons) impinge on a hydrogen cluster–jet target (thickness $\approx 2-3\times10^{14}$ atoms/cm^2), resulting in a luminosity of up to 10^{30} cm^{-2}s^{-1}. Data were collected for a total of about 60 hours of measurement.

The main trigger (Tr2) for the experiment was a single-particle trigger, generated by a particle hitting a counter in the first FD hodoscope plane and one of the two counters behind in the second plane. This trigger, selecting mainly single protons, was used with a prescaling factor 10. In parallel, the trigger from the silicon detector alone has been used (Tr3) in order to have the possibility of identifying quasi–elastic pp scattering for the deuteron vector polarisation measurements. A special trigger (Tr1), based on energy loss in the forward hodoscope [37], was used to identify ^{3}He particles to select events from the polarimetry reaction $\vec{d}p \to {}^3\mathrm{He}\,\pi^0$. A scaler trigger (Tr4) was used to read out the scalers periodically ten times per second. For each trigger signal (except Tr4), all subsystems of ANKE were read out. This includes the full forward system and the silicon telescope.

In order to establish the relative integrated luminosity of each of the polarisation states involved, we normalised the data using the beam current information. The signal from the beam current transformer (BCT) was fed into a voltage–to–

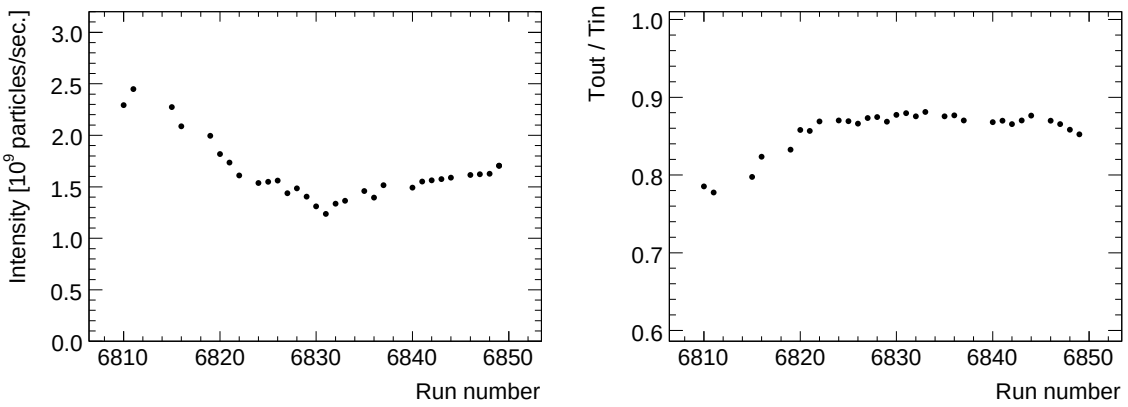

Figure 2.6: The beam intensity through the experiment (left panel) and corresponding deadtime behaviour (right panel).

frequency converter within the EDDA electronics and transformed into an optical signal to avoid deterioration. This information was transported to ANKE where, after conversion back to a NIM–signal, it was fed into the ANKE scaler system. In this way the BCT signal was available in the normal ANKE data stream for each of the polarisation states. The BCT signal is known to about 1%.

At the beginning of the experiment for the first few runs the beam intensity was roughly 3×10^9 *particles/sec*. Then it reduced down to 1.5×10^9 *particles/sec* and was stable until the end of the beam time (Fig. 2.6). The change of beam intensity affected also the efficiency of the DAQ system. With higher beam intensity the count rates were so high that the DAQ could accept only 80% of the triggers. Then it increased to about 88% and remained roughly constant for the rest of the experiment.

Chapter 3

Beam polarimetry

In order to measure the analysing powers of the CE–reaction we need to know the polarisation of the deuteron beam at our energy. Due to their much smaller anomalous magnetic moment, deuterons, unlike protons, do not have to cross any first–order depolarising resonances while being accelerated in COSY, where the typical working point tunes are 3.52 through 3.64 [22, 38]. It is therefore expected that there should be little or no loss of polarisation during acceleration and this has indeed been the experience over many years at the SATURNE synchrotron, which worked over a similar energy range [39]. Nevertheless, it is important to check that this is true at COSY.

The values of the deuteron beam polarisations provided by EDDA and LEP (see next section) can be checked by measuring a variety of nuclear reactions at T_d = 1170 MeV (p_d = 2400 MeV/c) using the ANKE spectrometer. This is the primary aim of this chapter.

3.1 Basic concept

The most general form for the cross section induced by spin–1 particles in the coordinate system of Fig. 3.1, may be written:

$$\left(\frac{d\sigma}{d\Omega}\right)_{pol} = \left(\frac{d\sigma}{d\Omega}\right)_0 \left(1 + 3/2 \sum_{i=1}^{3} p_i A_i + 1/3 \sum_{i,j=1}^{3} p_{ij} A_{ij}\right) \tag{3.1}$$

The small p represent the polarisation of the incident beam and A represent the analysing power of the reaction. In general, an incident beam may have all vector polarisation components: p_x, p_y and p_z. Because of parity conservation, the reaction is sensitive only to the components which are normal to the scattering plane. Similarly, although an incident beam may contain all six tensor polarisation components: $p_{zy}, p_{yz}, p_{xz}, p_{xx}, p_{yy}$ and p_{zz}, the reaction is sensitive, again because of parity, only to those indicated below:

$$\left(\frac{d\sigma}{d\Omega}\right)_{pol} = \left(\frac{d\sigma}{d\Omega}\right)_0 (1 + \frac{3}{2}\, p_y A_y + \frac{2}{3}\, p_{xz} A_{xz} + \frac{1}{6}\, p_{xx-yy} A_{xx-yy} + \frac{1}{2}\, p_{zz} A_{zz}) \quad (3.2)$$

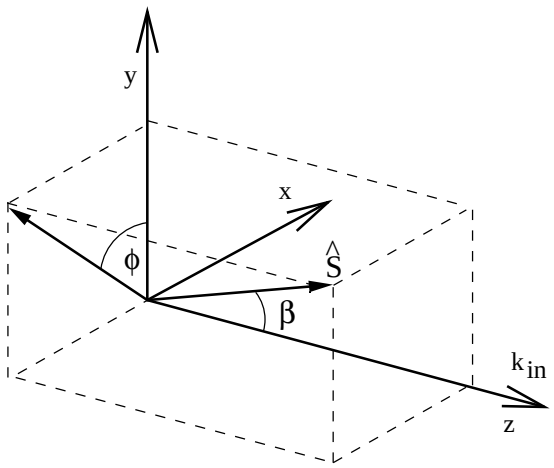

Figure 3.1: Madison convention for the definition of the laboratory-coordinate system, The scattering is in the x, z plane. The z axis is along the incident beam momentum.

The quantities defined are normalised so that the vector quantities (p_x, p_y, p_z and A_y) may vary between $+1$ and -1. The tensor quantities (p_{xy}, p_{yz}, p_{xz} and A_{xz}) may vary between $+\frac{3}{2}$ and $-\frac{3}{2}$, and tensor quantities ($p_{xx}, p_{yy}, p_{zz}, A_{xx}, A_{yy}$ and A_{zz}) may vary between $+1$ and -2.

For a polarised beam produced by an ion source, in the coordinate system of Fig. 3.1, the polarisation components are:

$$p_y = P_z \sin\beta\cos\phi \tag{3.3}$$
$$p_{xz} = -3/2\ P_{zz} \sin\beta\cos\beta\sin\phi \tag{3.4}$$
$$p_{xx-yy} = -3/2\ P_{zz} \sin^2\beta\cos 2\phi \tag{3.5}$$
$$p_{zz} = 1/2\ P_{zz}(3\cos^2\beta - 1) \tag{3.6}$$

We used a vertical alignment of the polarisation axis respect to the beam direction. Thus $\beta = 0$ and the differential cross section for the polarised deuteron beam can be expressed in the following form [40]:

$$\begin{aligned}\frac{d\sigma^{\uparrow}}{d\Omega}(\vartheta,\varphi) &= \frac{d\sigma_{\circ}}{d\Omega}(\vartheta)\{1+\frac{3}{2}P_z A_y(\vartheta)\cos\varphi \\ &\quad +\frac{1}{4}P_{zz}[A_{yy}(\vartheta)(1+\cos 2\varphi)+A_{xx}(\vartheta)(1-\cos 2\varphi)]\}\end{aligned} \tag{3.7}$$

Based on this equation, the only task is to extract the counts for the processes where the analysing powers are known. Besides the type of nuclear reaction, the analysing powers depend on the beam energy and the angle ϑ between the momentum k_{in} of incident and k_{out} outgoing particles. To determine the beam polarisation we compare counts from the polarised and unpolarised states.

3.2 Polarisations provided by LEP and EDDA

To assist in the optimisation of the polarisation of the beams inside COSY, a Low Energy Polarimeter (LEP, located in the injection beam line) consisting of a UHV chamber with eight flanges covered with thin stainless steel foils has been used [41]. The moveable target frame is equipped with viewers, allowing the adjustment of the beam position. A carbon target can be used for polarimetry measurements based on dC elastic scattering. It is possible to place detectors at azimuthal angles $\phi = 0°$, 90°, 180° and 270° in the ranges of polar angles 25° to 70° and 110° to 155°. NaI scintillators, directly coupled to photomultipliers, are used for particle identification.

The LEP is used at the COSY injection energy of $T_d = 75.6$ MeV ($p_d =$

539 MeV/c). Studies of the cross section, analysing power A_y, and the resulting figure of merit for 65 MeV [42] and 70 MeV [43] (Fig.3.2) deuterons suggest that the polarimeter should work best if the detectors are placed to accept polar angles near 40°. Unfortunately, under such conditions the tensor analysing powers are very small for this reaction so that the LEP is only sensitive to the vector polarisation of the beam [44]. Extrapolation of the published data [42, 43] to 75.6 MeV gives a value of $A_y(40°) = 0.61 \pm 0.04$.

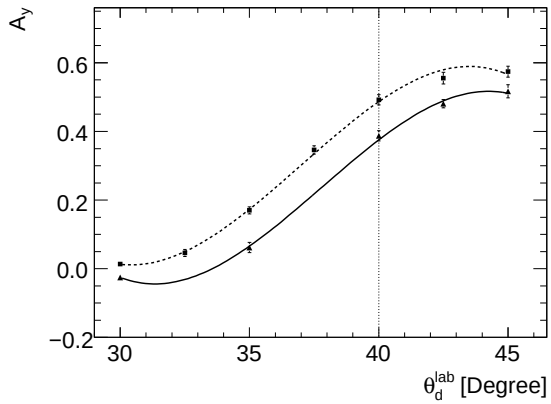

Figure 3.2: Analysing power *vs* deuteron laboratory angle for dC elastic scattering. The solid line represents the fit of data on 65 MeV and the dashed line for 70 MeV deuteron beam energy.

With the stable spin axis of the beam oriented along the y–direction, the number of particles scattered through a polar angle θ and an azimuthal angle ϕ, after corrections for beam luminosity, can be written as [40]

$$N(\theta,\phi) = N_0(\theta)\ \left[1 + \tfrac{3}{2}P_z A_y(\theta)\cos\phi + \tfrac{1}{4}P_{zz}\left\{A_{yy}(\theta)(1+\cos 2\phi) + A_{xx}(\theta)(1-\cos 2\phi)\right\}\right]. \tag{3.8}$$

The beam vector and tensor polarisations, P_z and P_{zz}, are labelled conventionally in the reference frame of the source, whereas the $\vec{d}\mathrm{C} \to d\mathrm{C}$ vector and tensor analysing powers, A_y and A_{yy}, refer to the reaction frame, where y is perpendicular to the plane of the COSY ring. Confining to the case of right (R) and left (L) counters placed at $\phi = 0°$ and 180°, respectively, this reduces to:

$$\begin{aligned} N_L(\theta) &= N_0(\theta)\left[1 + \tfrac{3}{2}P_z A_y(\theta) + \tfrac{1}{2}P_{zz}A_{yy}(\theta)\right] \\ N_R(\theta) &= N_0(\theta)\left[1 - \tfrac{3}{2}P_z A_y(\theta) + \tfrac{1}{2}P_{zz}A_{yy}(\theta)\right] \end{aligned} \tag{3.9}$$

Mode	P_z^{Ideal}	P_{zz}^{Ideal}	P_z^{LEP}	$P_z^{\text{LEP}}/P_z^{\text{Ideal}}$	P_z^{EDDA}	P_{zz}^{EDDA}
0	0	0	0.000 ± 0.010	—	0	0
1	$-\frac{2}{3}$	0	-0.572 ± 0.011	0.858 ± 0.017	-0.499 ± 0.021	0.057 ± 0.051
2	$+\frac{1}{3}$	+1	0.285 ± 0.011	0.855 ± 0.033	0.290 ± 0.023	0.594 ± 0.050
3	$-\frac{1}{3}$	–1	-0.302 ± 0.011	0.906 ± 0.033	-0.248 ± 0.021	-0.634 ± 0.051
4	$+\frac{1}{2}$	$-\frac{1}{2}$	0.395 ± 0.014	0.790 ± 0.028	0.381 ± 0.027	-0.282 ± 0.064
5	–1	+1	-0.758 ± 0.015	0.758 ± 0.015	-0.682 ± 0.027	0.537 ± 0.064
6	+1	+1	0.731 ± 0.014	0.731 ± 0.015	0.764 ± 0.027	0.545 ± 0.061
7	$-\frac{1}{2}$	$-\frac{1}{2}$	-0.417 ± 0.015	0.834 ± 0.030	-0.349 ± 0.027	-0.404 ± 0.065

Table 3.1: The table lists the eight configurations of the polarised deuteron ion source, showing the ideal values of the vector and tensor polarisations. The determinations of P_z^{LEP} were carried out at a momentum of 539 MeV/c using the Low Energy Polarimeter (LEP), The ratio of these to the ideal values are also given. The EDDA values of P_z^{EDDA} and P_{zz}^{EDDA} were obtained at 1042 MeV/c, assuming that state–0 was unpolarised. The systematic uncertainties of the polarisations P_z^{EDDA} and P_{zz}^{EDDA}, employed in the subsequent analysis, amount to ± 0.04.

Using the measured values of A_{yy} [42], together with an expected tensor polarisation of the deuteron beam of $P_{zz} \approx 0.6$, it is seen that the contamination of the measurement of the vector polarisation is on the percent level so that, to the desired level of accuracy, we can take

$$P_z = \frac{2}{3}\frac{1}{A_y}\left(\frac{N_L - N_R}{N_L + N_R}\right) \cdot \tag{3.10}$$

The results of the P_z measurements with the LEP for the different states are shown in Table 3.1. Also given are the ratios of P_z to the ideal polarisation that could be provided by the source for that state. The variation from 73% to 91% depends, among other things, on the number of RFTs involved.

After having measured the beam polarisation at the injection line, the accelerated beam polarisation was measured by EDDA. The EDDA detector has been used to provide a wealth of high quality polarised proton–proton elastic scattering data over a wide range of energies (0.5–2.5 GeV) by using a thin internal target and measuring during the energy ramp of the COSY accelerator [2]. With the same apparatus, elastic scattering of polarised deuterons from hydrogen was studied at $T_d = 270$ MeV ($p_d = 1042$ MeV/c) [45], where precise values are known for both

tensor and vector analysing powers [46]. In this way values of both vector and tensor polarisations of the circulating deuteron beam could be obtained at this energy.

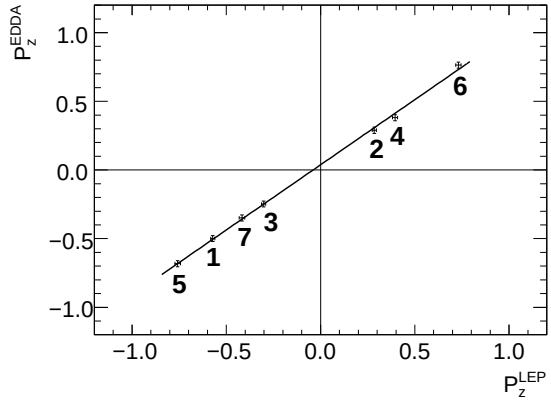

Figure 3.3: Comparison of the measurements of the vector polarisation of the deuteron beam from EDDA and LEP for the seven states of the source, listed in Table 3.1. The best fit straight line to the data is also shown. The uncertainty in the EDDA calibration results in a fit that does not cross the zero point exactly.

A fit to the data with the polarisations for all eight states being left as free parameters yields $P_z = -0.002 \pm 0.038$ for state–0. Any non–zero result might reflect a residual polarisation of state–0 or could be due to an instrumental asymmetry, *e.g.* caused by detector efficiencies. The data cannot distinguish between these two possibilities. Therefore, the EDDA values for the polarisations of the seven states shown in Table I, were extracted under the assumption that state–0 is unpolarised. Although supported by direct measurements with the LEP, the uncertainty of about ± 0.04 has to be considered as a systematic uncertainty on all the polarisations extracted using EDDA.

Since the EDDA and LEP data sets were taken with the same conditions in the source, in order to determine the systematic uncertainty of the polarisations, we compare quantitatively the two sets of results for P_z. This is done for the seven states in Fig. 3.3 using the data of Table 3.1. A linear fit of the two sets of results with $\chi^2/\mathrm{ndf} = 5.1/5$ gives $P_z^{\mathrm{EDDA}} = (1.05 \pm 0.02) P_z^{\mathrm{LEP}} + (0.038 \pm 0.008)$. The value of the offset constant is consistent with the uncertainty in the EDDA calibration, as shown by the ± 0.04 error bar in the polarisation of state–0. On the other hand, the 5% deviation of the slope from unity is similar to the precision in the absolute value of A_y used for the LEP. Thus, in addition to the statistical uncertainties shown

in Table 3.1, the polarisations P_z^{EDDA} and P_{zz}^{EDDA} have systematic errors of ± 0.04. The typical fractions of the ideal vector and tensor polarisations used later in the analysis of the ANKE results were $P_z = 74\%$ and $P_{zz} = 59\%$ respectively.

3.3 Measurements with ANKE

After being accelerated in the COSY ring [14], the values of the deuteron beam polarisations provided by EDDA and LEP can be checked by measuring various nuclear reactions at $T_d = 1170\,\mathrm{MeV}$ ($p_d = 2400\,\mathrm{MeV/c}$) using the ANKE spectrometer. The reactions that are pertinent to this polarisation study are:

The pion production reaction $\vec{d}p \to {}^3\mathrm{He}\,\pi^0$,

Quasi–free $\vec{n}p \to d\pi^0$ with a fast spectator proton,

Elastic scattering $\vec{d}p \to dp$ at small angles.

The first two reactions can be measured using foremost the information from the ANKE Forward Detector (FD) system [47, 48]. Though deuteron–proton elastic scattering can also be identified by using the FD information, coincidence measurements with the slow recoil proton being detected in a Silicon Tracking Telescope (STT) yield more precise information.

3.3.1 Identification of nuclear reactions

The ANKE experimental acceptance for charged particles as a function of the laboratory production angle and magnetic rigidity is shown on the left panel of the Fig. 3.4. From the loci of the kinematics of the four reactions that we investigated in this polarisation study it was seen that all of them had reasonable acceptances over some angular domain.

The main trigger used in the experiment consisted of a coincidence of different layers in the hodoscope of the FD. The ^{3}He were identified by means of a special energy loss trigger in the FD. In parallel, self–triggering of the STT was employed to identify unambiguously dp elastic scattering.

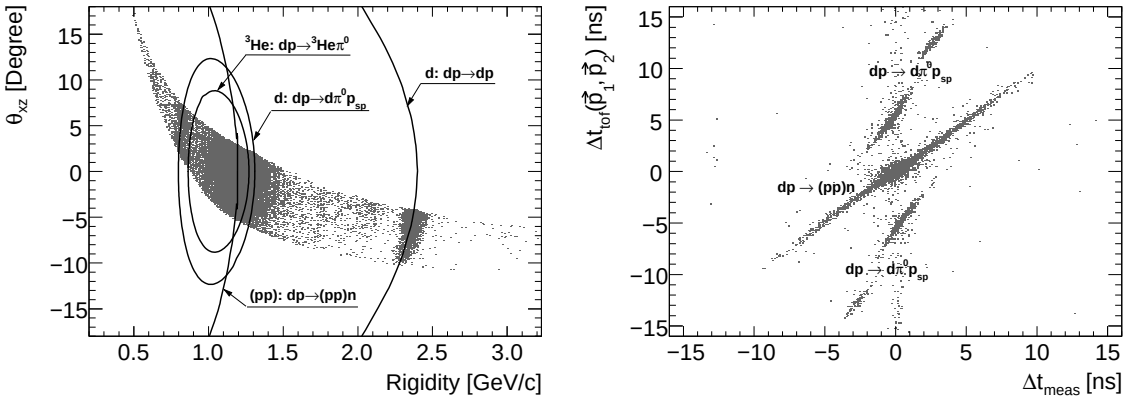

Figure 3.4: Left: ANKE experimental acceptance for four nuclear reactions of interest at a deuteron momentum of $p_d = 2400\,\mathrm{MeV/c}$. **Right:** Correlation of the measured time difference Δt_{meas} and the calculated $\Delta t_{\mathrm{tof}}(\vec{p_1}, \vec{p_2})$), assuming that the particle tracks correspond to protons.

Candidate events for different reaction channels can be identified in a plot of the time-of-flight difference between target and hodoscope (Δt_{meas}) versus the calculated time of flight difference ($\Delta t_{\mathrm{tof}}(\vec{p_1}, \vec{p_2})$), assuming the two particles hitting different hodoscope counters are protons, as shown on right panel of Fig. 3.4. Real proton pairs from the charge–exchange breakup $dp \to (pp)n$ are located along the diagonal of the scatter plot, where for illustration, it also shows how events from other reactions are transformed by this procedure.

3.3.2 $\vec{d}p \to {}^3\mathrm{He}\pi^0$ reaction

It is seen from Fig. 3.4 that there is a large acceptance for the $dp \to {}^3\mathrm{He}\,\pi^0$ reaction when the ^{3}He are emitted very close to the initial beam direction. In this region there are very detailed measurements of the sole non–vanishing deuteron (tensor) analysing power A_{yy} as a function of energy [49]. This reaction doesn't have a very high cross section and therefore it is hard to distinguish ^{3}He from the high rate protons and deuterons. For this purpose we implemented a third layer of scintillation hodoscopes and special trigger with a high energy threshold. ^{3}He is much heavier and slower compared to protons and deuterons, and thus we obtain a very good separation in the energy spectrum. The high–momentum branch of ^{3}He particles could be selected in the off–line analysis by applying two–dimensional cuts in ΔE versus momentum and Δt versus momentum for individual layers of the

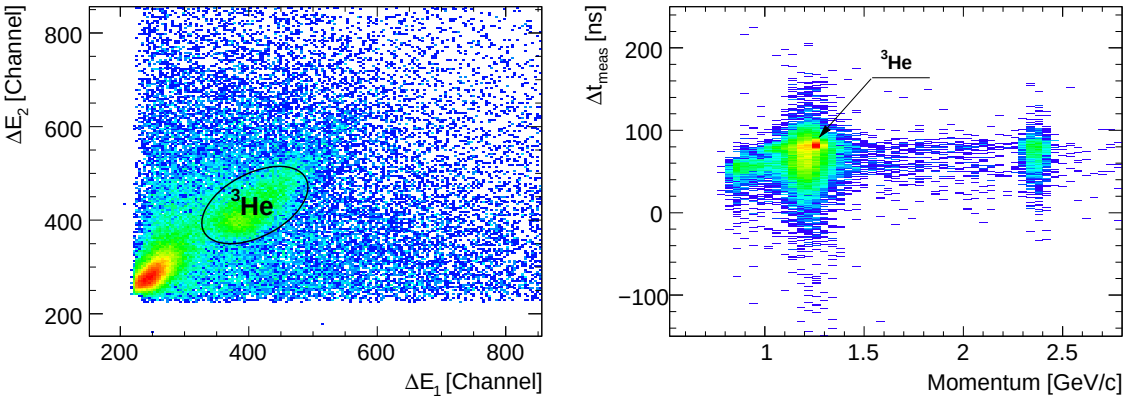

Figure 3.5: Left: Energy loss between two layers of hodoscope **Right:** Δt between 1st and 3rd layers versus momentum

forward hodoscope. The π^0 was identified through the missing–mass derived from the ^{3}He measurement, as described in Ref. [50]. The mean value of the missing mass distribution (Fig. 3.6) was close to the pion mass, with a stable background of less than 3%. Though the resulting peak has a large width, this is not critical since, apart from the radiative capture, there should be no physical background in this region, and no significant amount is seen in the figure.

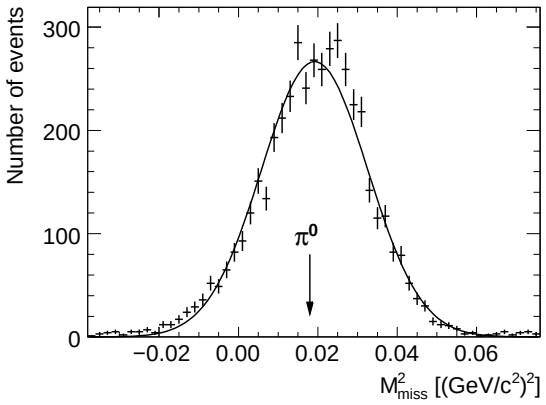

Figure 3.6: Missing–mass–squared for the $dp \to {}^3\mathrm{He}\,X$ reaction showing a Gaussian fit to a clearly identified π^0 peak.

The ANKE spectrometer is able to detect ^{3}He from the $dp \to {}^3\mathrm{He}\pi^0$ reaction in the angular range 0° to 25° in cm system. It has a large tensor analysing power and so is sensitive to the tensor polarisation of the beam. Unfortunately there is no vector analysing power measurement for this reaction at our energy. We have enough statistics to divide our acceptance into two angular ranges $0° < \theta^{cm}_{^3\mathrm{He}} < 12°$

and $12^\circ < \theta_{^3\mathrm{He}} < 25^\circ$ and compare the normalised counts with the calibrated polarisation (Fig. 3.7). The red points and lines show the initial data points and the fits for these two angular ranges. It is seen that for the higher angular range χ^2 gets worse. This can be an indication of a vector polarisation contribution, because we know that vector analysing power has a $\sin\theta$ dependence. We introduced arbitrary vector analysing powers for both angular ranges to get the smallest χ^2 (Fig.3.7, *green points and lines*). We obtained the $A_y(8^\circ_{cm}) = -0.036$ and $A_y(18^\circ_{cm}) = -0.070$ which agrees with our prediction about the possible vector polarisation contamination ($A_y \approx \alpha \sin\theta$).

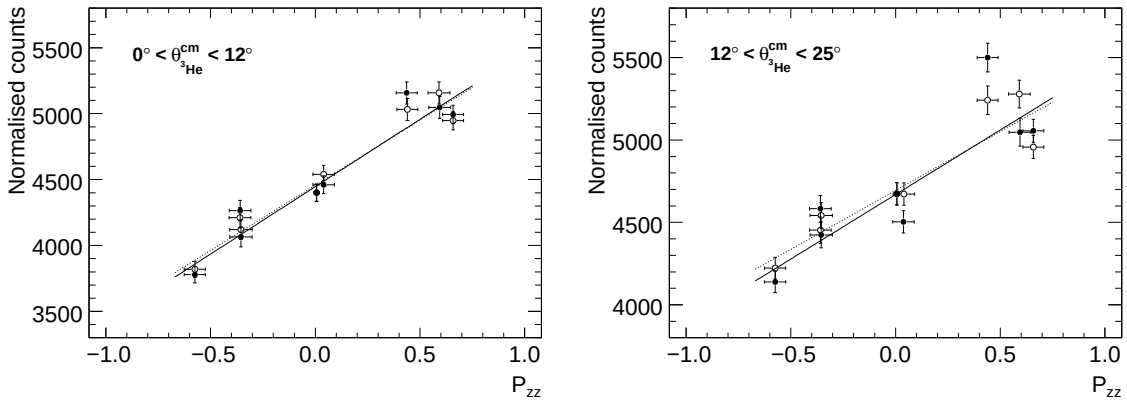

Figure 3.7: Normalised $dp \rightarrow {}^3\mathrm{He}\pi^0$ counts before (red) and after (green) correcting on vector polarisation factor, for two different angular range. **Left panel:** $\theta_{^3\mathrm{He}} = (0.0^\circ \div 12^\circ)$. **Right panel:** $\theta_{^3\mathrm{He}} = (12^\circ \div 25^\circ)$

The vector analysing powers at 0° are equal to zero. For the vector analysing power measurement we used the events near 0° where the average $\cos 2\varphi \approx 1$ and Eq.(3.7) will have the following form:

$$\frac{d\sigma^{\uparrow}}{d\Omega}(\vartheta,\varphi) = \frac{d\sigma_{\circ}}{d\Omega}(\vartheta)\left[1 + \frac{1}{2}P_{zz}A_{yy}(\vartheta)\right] \tag{3.11}$$

After correcting the counts in a $\pm 2.5\sigma$ missing–mass range, using the polarisation measurements from EDDA we find an analysing power of $A_{yy}(\theta = 0^\circ) = 0.461 \pm 0.030$, where the statistical and systematical uncertainties in the EDDA beam polarisations given in Table 3.1 have not been included. Interpolation of the SATURNE data to our energy leads to a value of $A_{yy}(\theta = 0^\circ) = 0.458 \pm 0.014$ [49].

3.3.3 Quasi–free $np \to d\pi^0$ reaction

In the bulk of reactions involving collisions with a deuteron at intermediate energies, the process is driven by the interaction with either the proton or neutron in the nucleus. The other particle is a *spectator*, a fact that has led to the extensive use of deuterium as a replacement for a free neutron target. In the case of a deuteron beam, a *spectator* proton (p_{sp}) would have roughly half the momentum of the beam. As seen from Fig. 3.4, ANKE has large acceptance for both the fast deuteron and the spectator proton, from the $dp \to p_{\rm sp}d\pi^0$ reaction. In the two-dimensional momentum spectrum of Fig. 3.8 are shown the bands arising from the high ($p_d \approx 1.3$ GeV/c) and low-momentum ($p_d \approx 0.8$ GeV/c) branches, corresponding to backward and forward production of the π^0 with respect to the beam direction.

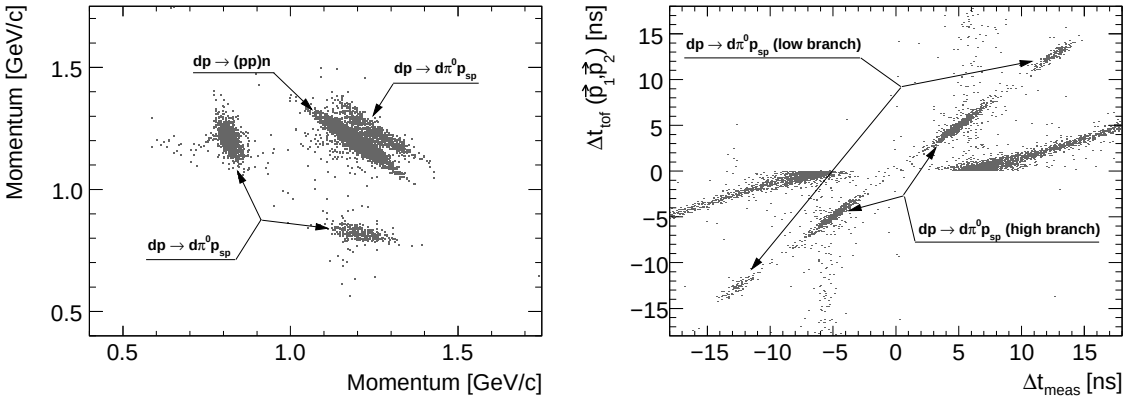

Figure 3.8: Left panel: Momentum correlation, and **Right panel:** Correlation of the measured time difference $\Delta t_{\rm meas}$ and the calculated $\Delta t_{\rm tof}(\vec{p_1}, \vec{p_2})$), assuming that the first particle track corresponds to a proton and second to a deuteron.

The first step in extracting quasi–free $\vec{n}p \to d\pi^0$ events from our data is to choose two–track events on the basis of the MWPC information. The momentum vectors were determined with the help of the magnetic field map of the spectrometer, assuming a point–like source placed in the centre of the beam–target interaction region. The smallness of the FD solid angle acceptance leads to a kinematic correlation for events with two or three particles in the final state. The $\vec{d}p \to p_{sp}dX$ candidates can be clearly identified from the correlation of the measured time difference $\Delta t_{\rm meas}$ and the calculated time of flight difference $\Delta t_{\rm tof}(\vec{p_1}, \vec{p_2})$ (see Fig. 3.8 right panel). As we see from the two–dimensional momentum distribution (Fig. 3.8 left panel) deuterons always have the same or smaller momentum than protons; therefore the

deuterons will arrive later thanto protons. In the $\Delta t_{\rm tof}(\vec{p_1}, \vec{p_2})$ calculation the slower particle was assumed to be a deuteron. The reaction shows up as a diagonal line in a two–dimensional plot for both the high deuteron momentum part (forward production in the cm system), and the low momentum region (backward production). After isolating these events we constructed the missing mass distributions, which correspond to the unobserved π^0 as clearly seen in Fig. 3.9.

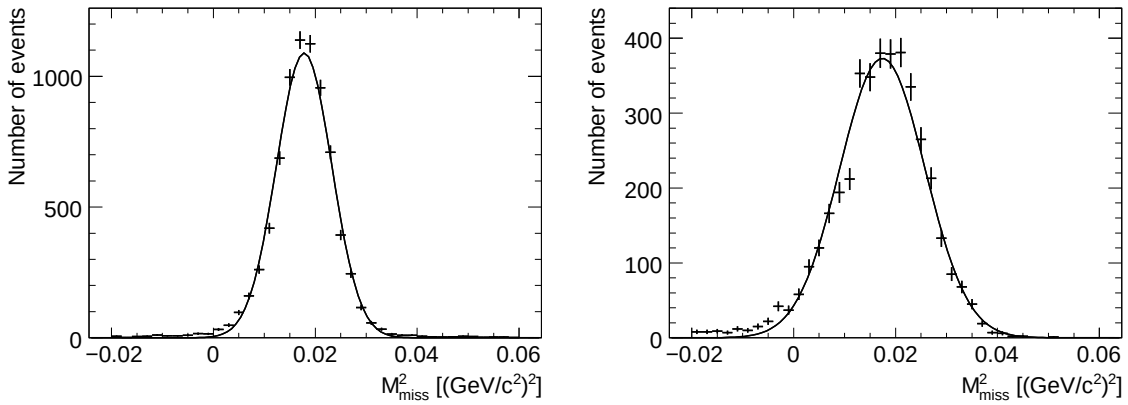

Figure 3.9: Left: Missing–mass–squared for the $dp \rightarrow p_{sp}dX$ reaction for the slow deuteron. **Right:** fast deuteron branches of the kinematics. In both cases Gaussian fits to the data are indicated.

Now it is well known that if one integrates over all Fermi momentum inside the deuteron the polarisation of a nucleon in the deuteron is reduced from that of the deuteron itself by a factor $P_z^n = \left(1 - \frac{3}{2}P_d\right) P_z^d$, where P_d represents the deuteron D-state probability. However, the D-state effects vanish like p_{sp}^2 at small spectator momenta and a negligible dilution is expected if we cut the data at $p_{sp} < 60$ MeV/c, and this condition is imposed in our subsequent analysis. The ranges of laboratory angles covered in the high and low branches are illustrated in Fig. 3.10 [3] and these show that they are in fact rather complementary regions.

Due to isospin invariance, the neutron analysing power in the $\vec{n}p \rightarrow d\pi^0$ reaction should be identical to the proton one in $\vec{p}p \rightarrow d\pi^+$, for which extensive compilations are available [3]. This is as expected for a quasi–free $np \rightarrow d\pi^0$ reaction and is sensitive only for vector polarisation. For this particular case the Eq. 3.7 will have following form:

$$\frac{d\sigma^{\uparrow}}{d\Omega}(\vartheta, \varphi) = \frac{d\sigma_{\circ}}{d\Omega}(\vartheta) \left(1 + \frac{3}{2} P_z A_y(\vartheta) \cos\varphi\right) \tag{3.12}$$

Using the known vector polarisation from EDDA and comparing polarised and un-

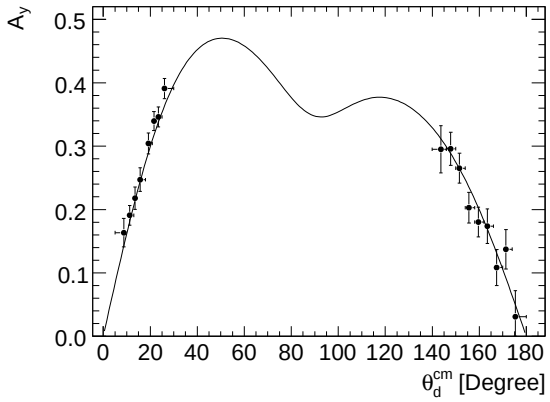

Figure 3.10: Analyzing power of the $\vec{n}p \to d\pi^0$ reaction measured at ANKE compared to the curve of values of A_y in $\vec{p}p \to d\pi^+$, as extracted from the SAID data base [3] (for numerical values, see Table 3.3.)

polarised states we were able to extract the analysing power for this process. As shown in Fig. 3.10, the agreement of our result with the SAID data base is very good for both large and small pion angles and this confirms the EDDA measurements of the vector polarisation of the deuteron beam. (Numerical results can be found in Table 3.3.) Within small error bars, there is no sign of any effect arising from the tensor polarisation of the deuteron beam.

3.3.4 Deuteron-Proton elastic scattering

It is obvious from Fig. 3.4 that deuteron–proton elastic scattering has a significant acceptance in ANKE. Due to its very high cross section, the fast deuterons from this process are clearly seen in the angle–momentum plot of Fig. 3.4 for laboratory polar angles from 5° to 10°. Since the locus of this reaction is well separated from those of the others, it is to be expected that the background should be very small. The proof of this can be found in Fig. 3.11 where, after selecting events from a broad region around the (p, θ_{xz}) locus, the missing mass with respect to the deuteron shows a proton peak with negligible background. As discussed below, the very different populations along the locus is merely a reflection of the rapid variation of the differential cross section with angle.

In contrast to the two reactions measured in ANKE that we have discussed thus far, $\vec{d}p$ elastic scattering depends strongly upon both the vector and tensor

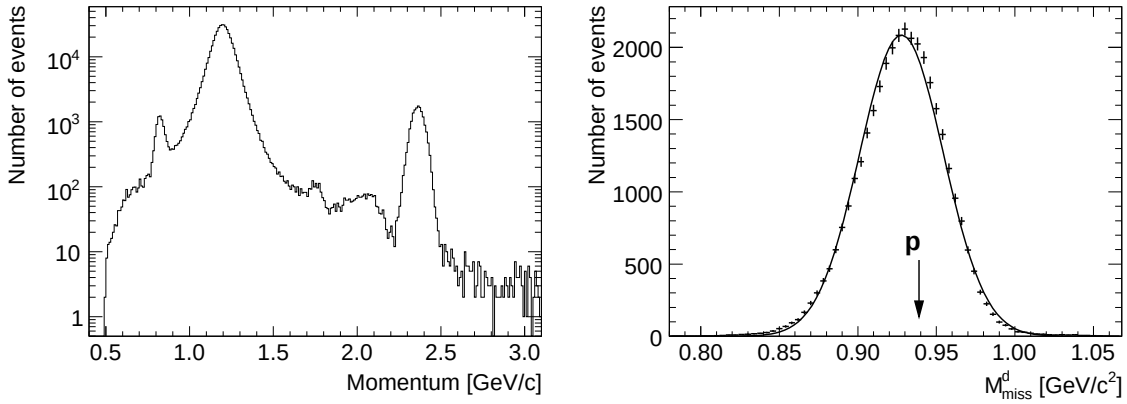

Figure 3.11: Left: Momentum distribution for single track events. **Right:** The missing mass of the deuteron for events that are close to the expected dp elastic locus in Fig. 3.4. There is little or no background under the proton peak, which has a width of $\sigma = 27$ MeV/c^2.

polarisations of the deuteron beam. Fortunately the analysing powers A_y, A_{yy}, and A_{xx} of this reaction have been measured at Argonne [51] for $T_d = 1194$ MeV and SATURNE [39] for $T_d = 1198$ MeV. The EDDA polarimeter [2] is based upon the same reaction, but the ANKE acceptance in the azimuthal angle ϕ is insufficient to allow us to extract the analysing powers for each state. Hence, only global values can be given on the basis of the EDDA measurement.

Our ϕ coverage is sufficient to extract values for A_y, as shown in Fig. 3.12 (left panel). Comparing with the Argonne and SATURNE results, the agreement is very good, with all points coinciding within the published statistical errors. The situation is not quite as clean in the case of the tensor analysing power since, by retaining events in the acceptance range $167^\circ < \phi < 193^\circ$, there is some small contamination of the A_{xx} signal contained within our A_{yy} measurements. We therefore introduced a correction of about 4% to account for this effect using information derived from the ratio A_{xx}/A_{yy} determined at Argonne [51], where it should be noted that this ratio does not depend on the beam polarisation used in their analysis. The agreement presented in Fig. 3.12 (right panel) is very satisfactory; Numerical values of A_y and A_{yy} are given in Table 3.3.

Though the events identified from the FD information shown in Fig. 3.11 are very clean, some of the systematics of the experiment can be checked from the data where the slow recoil proton from the $\vec{d}p \to dp$ elastic scattering was detected in the silicon telescope in coincidence with the deuteron in the FD. Although this restricts

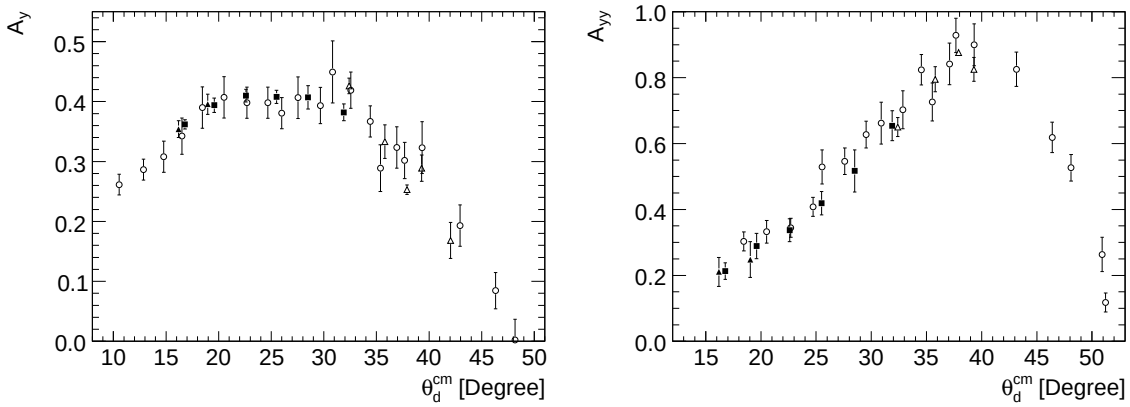

Figure 3.12: Vector (left panel) and tensor analysing powers (right) for elastic deuteron–proton scattering at small forward angles. Our data at 1170 MeV (solid squares) were obtained using information solely from the forward detector system whereas two points (solid triangles) resulted from coincidence measurements with the silicon telescope (for numerical values, see Table 3.3). These data are compared to the results from Argonne at 1194 MeV [51] (open circles) and SATURNE at 1198 MeV [39] (open triangles). It should be noted that the tensor beam polarisation at SATURNE was the subject of a series of very careful calibrations.

both the acceptance and the statistics, the determination of the angles and the total lack of any background present in principle many advantages. However, as shown in the figure, the results hardly change when this coincidence is introduced.

3.4 Precision of the ANKE results

The numerical results from the measurements described in this section are given in Table 3.3. We here discuss separately the precisions with which each of the reactions determines one of the beam polarisations with the aim of extracting the best values and errors for P_z and P_{zz} at 1170 MeV. This will also allow us to put limits on the amount of depolarisation by the beam through acceleration to this energy.

Though the $\vec{d}p \to {}^3\mathrm{He}\,\pi^0$ reaction in the forward direction has a significant tensor analysing power signal, the statistical error achieved so far at ANKE does not allow us to make a strong statement on the basis of these results. Comparing with the precise results from SATURNE [49], we find that

$$A_{yy}(\text{ANKE}) = (1.01 \pm 0.07)\, A_{yy}(\text{SATURNE})\,. \tag{3.13}$$

The $\vec{n}p \to d\pi^0$ reaction is only sensitive to the vector polarisation of the beam. We find that the analysing power at different angles is proportional to the SAID prediction for $\vec{p}p \to d\pi^+$ [3] with

$$A_y(\text{ANKE}) = (1.03 \pm 0.02)\, A_y(\text{SAID})\,, \tag{3.14}$$

where $\chi^2/ndf = 10.5/16$. Although the SAID database does not allow one to extract errors, the numerous experiments in this range suggest an overall precision of about 3% [52]. Allowing also for a possible small violation of charge independence that links the $\vec{n}p \to d\pi^0$ and $\vec{p}p \to d\pi^+$ analysing powers, a very conservative estimate on the error in P_z from this reaction is about 5%.

Elastic deuteron–proton scattering is sensitive to the vector and tensor polarisations of the beam. Comparing our measurements of A_y for $\vec{d}p \to dp$ with those of Argonne [51] shown in Fig. 3.12 (left), the average over the points near the maximum yields

$$A_y(\text{ANKE}) = (1.00 \pm 0.03)\, A_y(\text{Argonne})\,. \tag{3.15}$$

Unlike the case for the vector analysing power of $\vec{d}p \to dp$, there are clear discrepancies between the measurements of Argonne [51] and SATURNE [39] for the tensor analysing power A_{yy} shown in Fig. 3.12 (right), with the latter being $6\% \pm 3\%$ lower. This was remarked upon in the SATURNE paper and great care was then taken to establish very accurate values of the beam polarisations. Using the SATURNE and renormalized Argonne values, we find for this reaction that

$$A_{yy}(\text{ANKE}) = (0.99 \pm 0.06)\, A_{yy}(\text{SATURNE})\,. \tag{3.16}$$

However, for neither of the two analysing powers have we tried to include corrections for the small differences in beam energy between the different experiments.

Putting all these results together, we see that

$$\begin{aligned} A_y(\text{ANKE}) &= (1.01 \pm 0.03)\, A_y(\text{Expected})\,, \\ A_{yy}(\text{ANKE}) &= (0.99 \pm 0.03)\, A_{yy}(\text{Expected})\,. \end{aligned} \tag{3.17}$$

The error bars on the "Expected" results are obtained from theory and a variety of experiments around 1170 MeV. However, they do not explicitly include the uncertainties of 2.1% and 2.6% in the SATURNE values of P_z and P_{zz}. If one takes these into account then the uncertainties in the vector and tensor polarisations of the deuteron beam in ANKE are both on the 4% level.

The central values shown in Eq. (3.17) reflect the possible loss of polarisation during the acceleration of the deuterons from the EDDA energy to that of ANKE. Though these indicate very little depolarisation, one cannot draw very tight limits on this effect because of the uncertainties introduced by the calibration of the EDDA polarimeter. Taking just the systematic errors of 4% here, we suggest that any polarisation loss is below 6% for both the vector and tensor parameters.

T_d (GeV)	$T_{20}(0^\circ)$	$T_{20}(180^\circ)$
0.40	-1.336 ± 0.016	-1.336 ± 0.016
0.41	-1.435 ± 0.010	-1.035 ± 0.015
0.45	-1.377 ± 0.008	-0.216 ± 0.031
0.50	-1.416 ± 0.015	-0.738 ± 0.049
0.60	-1.257 ± 0.015	-1.333 ± 0.035
0.65	-1.166 ± 0.014	-1.440 ± 0.026
0.70	-1.085 ± 0.010	-1.335 ± 0.051
0.80	-0.889 ± 0.010	-0.451 ± 0.034
0.90	-0.779 ± 0.023	0.251 ± 0.051
1.00	-0.650 ± 0.007	0.292 ± 0.023
1.10	-0.636 ± 0.019	0.236 ± 0.048
1.20	-0.670 ± 0.016	0.071 ± 0.044
1.30	-0.676 ± 0.027	-0.156 ± 0.066
1.40	-0.729 ± 0.023	-0.240 ± 0.081
1.50	-0.784 ± 0.029	-0.342 ± 0.064
1.60	-0.771 ± 0.028	-0.384 ± 0.086
1.70	-0.756 ± 0.016	-0.300 ± 0.066
1.75		-0.390 ± 0.077
1.80	-0.803 ± 0.026	-0.457 ± 0.151
1.85		-0.485 ± 0.114
1.90	-0.905 ± 0.033	-0.916 ± 0.080
1.95		-0.770 ± 0.093
2.00	-0.953 ± 0.029	-0.445 ± 0.075
2.10	-0.938 ± 0.036	-0.484 ± 0.118
2.20	-1.103 ± 0.051	-0.638 ± 0.114

Table 3.2: Analysing powers T_{20} and T_{22} of the $\vec{d}p \rightarrow {}^3\mathrm{He}\,\pi^0$ reaction as a function of beam energy, for forward and backward scattered ^{3}He measured at SATURNE [49].

$\vec{d}p \to dp$	θ^d_{cm}	A_y	A_{yy}
FD	16.8°	0.362 ± 0.008	0.212 ± 0.025
	19.6°	0.394 ± 0.012	0.289 ± 0.039
	22.6°	0.410 ± 0.011	0.337 ± 0.034
	25.5°	0.408 ± 0.011	0.419 ± 0.035
	28.5°	0.407 ± 0.020	0.517 ± 0.064
	31.9°	0.382 ± 0.014	0.654 ± 0.045
FD+STT	16.2°	0.354 ± 0.014	0.209 ± 0.044
	19.1°	0.395 ± 0.017	0.248 ± 0.054
$\vec{n}p \to d\pi^0$	θ^d_{cm}	A_y	A_y(SAID)
	8.7°	0.164 ± 0.023	0.142
	11.3°	0.191 ± 0.015	0.181
	13.5°	0.218 ± 0.018	0.214
	15.7°	0.247 ± 0.019	0.244
	19.4°	0.303 ± 0.017	0.292
	21.6°	0.340 ± 0.015	0.318
	23.4°	0.346 ± 0.016	0.337
	26.1°	0.391 ± 0.016	0.364
	143.8°	0.295 ± 0.037	0.311
	147.8°	0.296 ± 0.026	0.289
	151.6°	0.265 ± 0.024	0.265
	155.6°	0.203 ± 0.024	0.236
	159.6°	0.180 ± 0.023	0.203
	163.4°	0.174 ± 0.027	0.170
	167.4°	0.109 ± 0.028	0.132
	171.3°	0.137 ± 0.031	0.092
	175.3°	0.031 ± 0.041	0.050
$\vec{d}p \to {}^3\mathrm{He}\,\pi^0$	$\theta^{^3\mathrm{He}}_{cm}$		A_{yy}
ANKE	0°		0.461 ± 0.030
SATURNE	0°		0.458 ± 0.014

Table 3.3: Analysing powers A_y and A_{yy} of the $\vec{d}p \to dp$ reaction as a function of θ^d_{cm} (top, using only the FD, or a coincidence of FD and STT), analysing power A_y of the $\vec{n}p \to d\pi^0$ reaction as function of θ^d_{cm} (middle), and the values of the analysing power A_{yy} of the $\vec{d}p \to {}^3\mathrm{He}\,\pi^0$ reaction at $\theta^{^3\mathrm{He}}_{cm} = 0°$ from ANKE and SATURNE [49] (bottom). Also shown are the SAID predictions for $A_y(\vec{p}p \to d\pi^+)$ obtained using the SP96 solution [3].

Chapter 4

Luminosity determination

In order to extract the cross section for the $dp \to (pp)n$ reaction, the absolute value of the luminosity must be determined. Luminosity L relates the cross section σ of a given physical process to its corresponding event rate, R:

$$R = L \times \sigma \tag{4.1}$$

Therefore, by definition, L is a process-independent quantity which is completely determined by the properties of the beam and target. There are different types of luminosity measurement. The method which we used in our data analysis relies on accurately measuring the rate of a well-known and sizeable cross section, whereupon L is determined from the expression (4.1)

The measurement of the luminosity has been done using the quasi–free $dp \to d\pi^0 p_{sp}$ reaction. The detection of a spectator proton in coincidence with the deuteron, produced *via* $np \to d\pi^0$, closely matches the acceptance for the two charge-exchange protons. Some check on luminosity could be provided through the study of elastic deuteron-proton scattering, though there are larger uncertainties in the relevant World database.

4.1 Luminosity determination by quasi-free $np \to d\pi^0$

As described in section 3.3.3, ANKE has a large acceptance for both the fast deuteron and the spectator proton, $p_{\rm sp}$, from the $dp \to p_{\rm sp} d\pi^0$ reaction. Both of these particles have momenta that are very similar to those of the two protons in the $dp \to (pp)n$

reaction. Any error in the estimation of the two-particle acceptance will therefore tend to cancel between the two reactions. Interpreting the data in terms of quasi–free pion production, $np \to d\pi^0$, the counting rates for the $dp \to p_{\rm sp}d\pi^0$ reaction will allow a useful evaluation of the luminosity to be made. In order to ensure that the kinematics are similar to the two protons from the charge exchange at low E_{pp}, in addition to the extraction procedure described in 3.3.3 a cut is made on the difference between the momenta of the assumed proton and deuteron of $\Delta p < 175$ MeV/c. An analogous cut was placed upon the simulation of the acceptance.

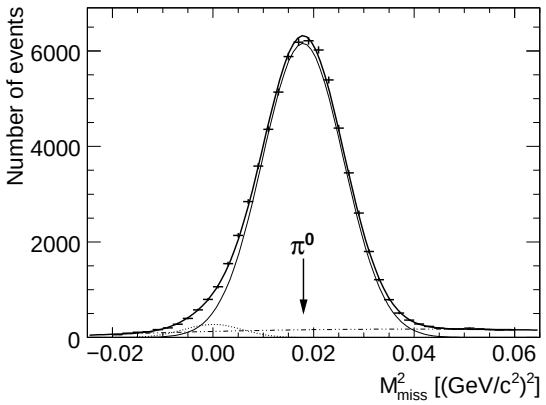

Figure 4.1: Missing–mass–squared distribution for the $dp \to p_{\rm sp}dX$ reaction for the fast deuteron branch of the kinematics. A fit to the data with a Gaussian and a constant background is indicated. Some of the event excess for $M^2_{\rm miss} \approx 0$ might be associated with the quasi–free $np \to d\gamma$ reaction.

The $dp \to p_{\rm sp}d\pi^0$ identification is completed by studying the missing mass of the reaction with respect to the final dp pair, as shown in Fig. 4.1. The Δp cut means that only events corresponding to the forward deuteron branch are presented here. As is seen from Fig. 3.4, these ones have similar acceptance to those of the $dp \to (pp)n$ reaction. The data show a very prominent π^0 peak though there is evidence for background on the low $M^2_{\rm miss}$ side, some of which might arise from the quasi–free $np \to d\gamma$ reaction.

It is not possible to detect all events from the $np \to d\pi^0$ process due to ANKE geometrical restrictions. Thus we must correct the counts on the ANKE acceptance. The acceptance was calculated using a GEANT-based simulation program that includes a realistic description of the set-up. To confirm the spectator hypothesis, a Monte Carlo simulation has been performed within PLUTO [53], using the Fermi momentum distribution evaluated from the Paris deuteron wave function [54]. As is

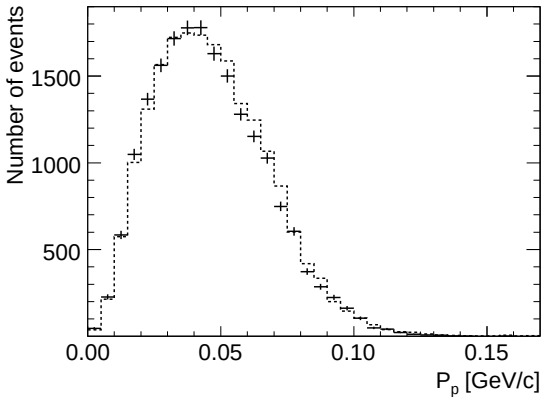

Figure 4.2: Momentum distribution of the fast proton from the $dp \to p_{\rm sp}d\pi^0$ reaction transformed into the rest frame of the initial deuteron (histogram). The simulation (crosses) uses the Fermi momentum distribution obtained from the Paris deuteron wave function [54]. Only data with $p_{\rm sp} < 60$ MeV/c were used in the luminosity evaluation.

clear from Fig 4.2, the data are completely consistent with quasi-free production on the neutron leading to a spectator proton. However, in order to reduce further possible contributions from multiple scattering *etc.*, only events with $p_{\rm sp} < 60$ MeV/c were retained for the luminosity evaluation. The numbers of events were then corrected for acceptance and data acquisition efficiency *etc.* and are presented in 0.25° bins of deuteron laboratory angle in Fig. 4.3.

Isospin invariance requires that the differential cross section for $np \to d\pi^0$ should be half that of the $pp \to d\pi^+$ reaction, for which there are many measurements and an extensive data compilation by the SAID group [55]. Predictions of the SAID program reproduce well the shape of the data in Fig. 4.3 and, after scaling this to agree with our experimental points, the luminosity can be deduced. It is of course possible that there could be small isospin violations between π^0 and π^+ production which may introduce uncertainties in the luminosity on the very few per cent level.

4.2 Luminosity determination by *dp* elastic scattering

An alternative way of determining the luminosity required to evaluate the charge–exchange cross section would be through the measurement of deuteron–proton elastic scattering using data from the unpolarised spin mode. At the ANKE experiment,

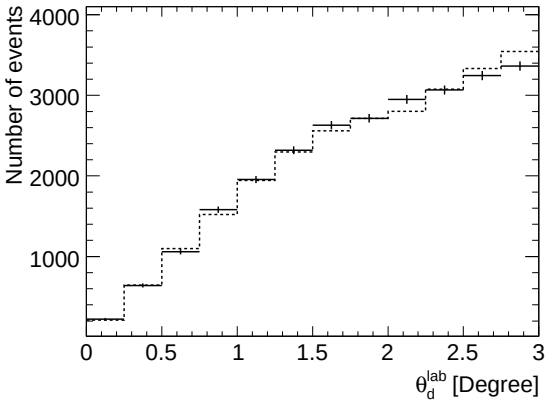

Figure 4.3: Corrected numbers of counts of quasi–free $np \to d\pi^0$ events in 0.25° bins (crosses). The histogram represents the prediction of the $pp \to d\pi^+$ differential cross section taken from the SAID program [55]. After taking an isospin factor of two into account, scaling the simulation to agree with the experimental points allows the luminosity to be evaluated.

only a small fraction of elastically scattered deuterons can be detected, mainly due to the geometrical restrictions. Fig. 4.4 shows the angular acceptance of the ANKE spectrometer for this reaction. It is clearly seen that the distribution is symmetrical with the respect to the azimuthal angle. Having cleanly identified good *dp*

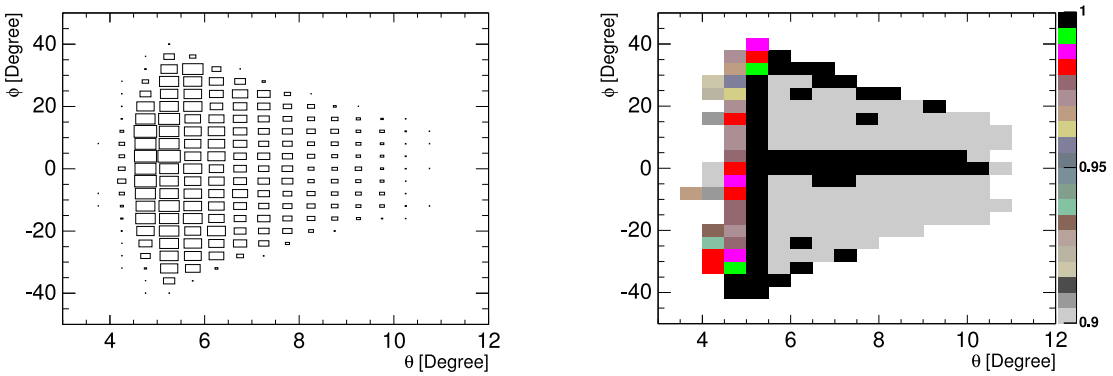

Figure 4.4: Left: Efficiency corrected two-dimensional histogram of event distribution over the polar and azimuthal angular range. **Right:** Efficiency map for the forward MWPCs used for luminosity determination.

elastic scattering events (Sec. 3.3.4), their numbers were corrected for the MWPC efficiency. For this purpose, two–dimensional efficiency maps were created for each plane (Fig.4.4) and the tracks weighted using these maps. The events were grouped into laboratory polar angular bins of width 0.5° in order to plot the angular distri-

bution. The numbers in each bin were adjusted by the prescaling factor using the correction of the DAQ efficiency. For each polar angular bin (i), the detector solid angle (Ω_i^{det}) calculation has been done using the formula:

$$\Omega_i^{det} = \Delta\phi_i[\cos\theta_i - \cos(\theta_i + 0.5^\circ)] \tag{4.2}$$

Here the $\Delta\phi_i$ (the edges for azimuthal angles) for each angular bin was defined experimentally using the typical spectra for azimuthal angular distributions (Fig. 4.5.

The corrected numbers of events are plotted as a function of the deuteron laboratory angle in Fig. 4.6. However, in order to avoid regions where there is a strong azimuthal variation in the acceptance, only the range $5.5^\circ < \theta_{xz} < 9.5^\circ$ was retained for the luminosity estimation.

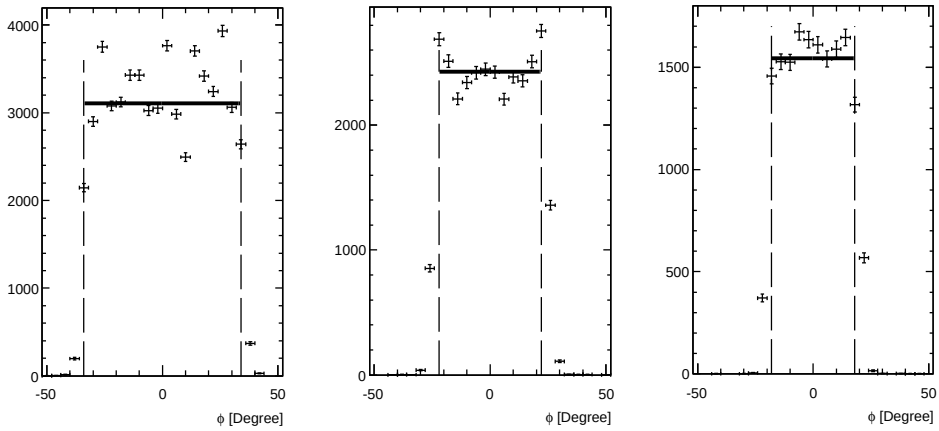

Figure 4.5: Typical histograms of the azimuthal angular distributions to define the detector edges (vertical lines) in the azimuthal direction, for several θ bins (5.5° - 6.0°, 6.5° - 7.0° and 8.5° - 9.0°)

Very close to our energy ($T_d/2 = 585$ MeV) elastic proton–deuteron scattering has been measured at 582 MeV using carbon and deuterated polyethylene targets together with counter telescopes [56]. The differential cross sections were then obtained from a CD_2–C subtraction. The resulting values, transformed to the proton rest frame, are also shown in Fig. 4.6. Although the absolute normalisation was established well using the carbon activation technique, it should be noted that a test measurement at one angle, where a magnetic spectrometer was used to suppress background from breakup protons, led to a cross section that was 10% lower,

though with a significant statistical error. There is therefore the possibility that these data include some contamination from non-elastic events. Despite this uncertainty, the comparison of the two data sets allows a value of the luminosity to be deduced for our experiment.

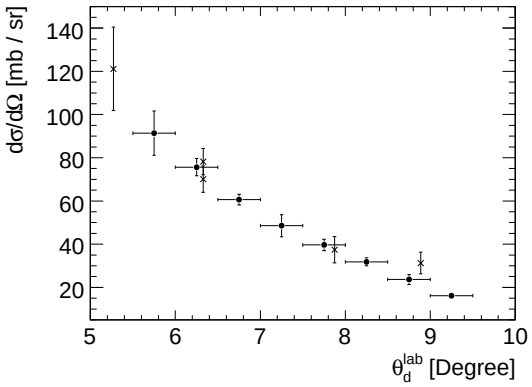

Figure 4.6: Laboratory differential cross section for small angle dp elastic scattering in 0.5° bins (circles) are compared to the $pd \to pd$ values reported in Ref. [56] and transformed to the proton rest frame (crosses). By scaling our data to agree with these values, an estimate of the luminosity could be made. Only data in the range $5.5° < \theta_d^{\rm lab} < 9.5°$ were used for this purpose.

The only other available data close to our momentum ($p_d = 2.4$ GeV/c) comes from a measurement of deuteron–proton elastic scattering in a hydrogen bubble chamber experiment at ten momenta between 2.0 and 3.7 GeV/c [57]. Although numerical values are not available, the results show a smooth variation with beam momentum when plotted as a function of the momentum transfer t. Interpolating these results to 582 MeV, the data seem to be consistent with those of Ref. [56], though the variation of the cross section with t is extremely strong.

4.3 Luminosity result

Having determined the luminosity independently on the basis of the $dp \to dp$ and quasi–free $np \to d\pi^0$ measurements, the results are compared in Fig. 4.7 for all the individual "good" runs. The luminosity ratio is consistent with being constant,

$$\mathcal{L}(dp \to dp) / \mathcal{L}(np \to d\pi^0) = 0.80 \pm 0.01 \qquad (4.3)$$

where the error is purely statistical. The smallness of the fluctuations in Fig. 4.7 implies that the two methods are sensitive to the same quantity, though with a different overall normalisation. Of the 20% discrepancy, about 5% can be accounted for by the shadowing correction [58], which reduces slightly the quasi–free cross sections on the deuteron compared to their free values. To a first approximation the deuteron charge exchange would be subject to a rather similar shadowing correction. Some of the residual difference might be due to inelastic events in the published data [56].

Apart from the sparsity of the World data set on $dp \to dp$ compared to that on $pp \to d\pi^+$, it should be noted that the elastic deuteron–proton differential cross section varies very rapidly with angle. A shift of a mere 0.1° in the deuteron laboratory angle induces a 5% change in the cross section. This is to be compared to the absolute precision in the angle determination in ANKE, which is $\approx 0.2°$. For these reasons much more confidence can be ascribed to the quasi-free $np \to d\pi^0$ method to determine the luminosity. The final number for the integrated luminosity for all good runs was:

$$\mathcal{L} = (12.5 \pm 0.5)\ nb^{-1}.$$

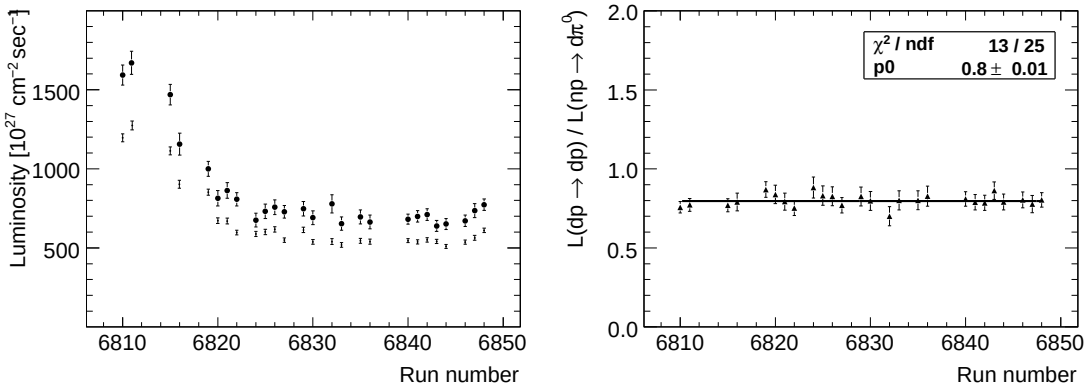

Figure 4.7: Left: Luminosity versus run number. Circles represents the luminosity determined using the $np \to d\pi^0$ reaction. Squares are the luminosity from $dp \to dp$ reaction. **Right:** Ratio of the luminosity determined from small angle deuteron–proton elastic scattering and quasi–free $np \to d\pi^0$ pion production *versus* the individual run number.

Chapter 5

Charge–exchange reaction

The measurement of the cross-section and the analysing power was performed at beam energy $T_d = 1.170$ GeV as a function of transferred momentum q. To check the behaviour of these observables, several cuts on the excitation energy E_{pp} were applied. In this chapter the extraction of differential cross–sections and analysing powers are described. The proof of principle achieved here for the method used suggests that measurements at higher energies will provide useful information in regions where the existing np database is far less reliable.

5.1 Differential cross section

In the previous chapter we have discussed the luminosity determination with two different reactions. This was the preparatory work for the cross-section determination. In addition to all efficiency corrections (DAQ, detector system) we have to correct for the experimental acceptance to obtain the real number of CE counts. But before that, one needs a clear identification of the reaction itself, which we haven't discussed up to now. These two major steps, together with the luminosity obtained from the $np \to d\pi^0$ reaction, will allow the differential cross section determination.

5.1.1 Reaction identification

In the deuteron charge–exchange reaction, two fast protons are emitted in a narrow forward cone with momenta around half that of the deuteron beam. The detection of

proton pairs was already successfully exploited during earlier measurements [35, 59]. Such coincident pairs can be clearly identified using information from the FD system in much the same ways as for the $p_{sp}d\pi^0$ reaction of Sec. 3.3.3. Having measured the momenta of two charged particles, their times of flight from the target to the hodoscope were calculated assuming that these particles were indeed protons. The difference between these two times of flight was compared with the measured time difference for those events where the particles hit different counters in the hodoscope (Fig. 5.1). This selection, which discarded about 20% of the events, eliminated almost all the physics background, for example, from dp pairs associated with π^0 production. The resulting missing–mass distribution for identified ppX events shows a clean neutron peak in Fig. 5.1 at $M_X = (940.4 \pm 0.2)$ MeV/c^2 with a width of $\sigma = 13$ MeV/c^2, sitting on a slowly varying 2% background.

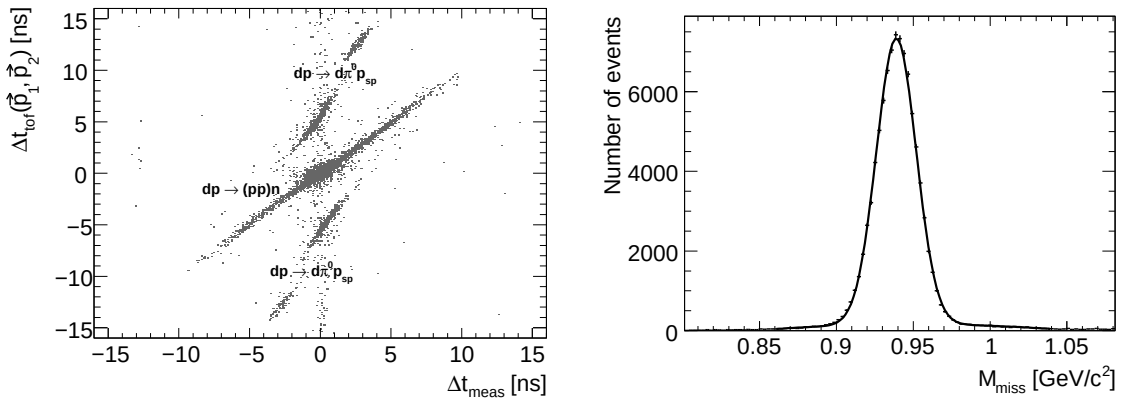

Figure 5.1: Left: Correlation of the measured time difference $\Delta t_{\rm meas}$ and the calculated $\Delta t_{\rm tof}(\vec{p_1},\vec{p_2})$), assuming that the particle tracks correspond to protons. **Right:** Missing mass distribution for proton pairs selected by the TOF criterion described in the text. A fit to the data in terms of a Gaussian plus a smoothly varying background shows the latter to be at about the 2% level. The central value agrees with the neutron mass to within 0.1%. Events falling within $\pm 2.5\sigma$ of the peak position were retained in the analysis.

5.1.2 Acceptance calculation

The kinematics of a $2 \rightarrow 3$ particle reaction is defined by 5 independent variables. To simulate the process we chose the following ones:

- E_{pp} – the excitation energy of the two protons.

- $\cos\theta_{pp}^{cm}$ – the cosine of the polar angle of the proton pair (di–proton) in the overall cm system.
- ϕ_{pp}^{cm} – azimuthal angle of the proton pair (di–proton) in the overall cm system.
- $\cos\theta_{k}^{cm}$ – the polar angle of the one proton in cm system of two protons.
- ϕ_{k}^{cm} – azimuthal angle of the one proton in cm system of two protons.

Since the counting rate varies rapidly with both E_{pp} and $\cos\theta_{pp}^{cm}$, the acceptance was estimated by inserting the predictions of the impulse approximation model into the Monte Carlo simulation in a two–dimensional grid. We generated 10^8 events and each of these was transformed in the laboratory system and then traced through ANKE using the GEANT simulation program that includes the realistic description of the D2 dipole and FD system. To have the equivalent with the experimental conditions, the accidental background was also produced. Using the MWPC information the tracks and corresponding momenta were reconstructed using the same track and momentum reconstruction programs. The acceptance correction as a function of these five variables $A\left(E_{pp}, \cos\theta_{pp}^{c.m.}, \phi_{pp}^{c.m.}, \cos\theta_{k}^{c.m.}, \phi_{k}^{c.m.}\right)$, was calculated by dividing the number of detected events by the number of generated events

$$A\left(E_{pp}, \cos\theta_{pp}^{c.m.}, \phi_{pp}^{c.m.}, \cos\theta_{k}^{c.m.}, \phi_{k}^{c.m.}\right) = \frac{N_{det}}{N_{tot}} \tag{5.1}$$

Only at small momentum transfer and small pp excitation energy is the ANKE geometric acceptance even approximately isotropic. Unlike the case of $dp \to p_{\rm sp}d\pi^0$ used for the luminosity determination, one cannot limit the data selection to this small region of phase space. Figure 5.2 shows the distribution of unpolarised charge–exchange events for $E_{pp} < 3$ MeV in terms of the azimuthal angle of the diproton ϕ_{pp} in the overall cm system. This variable is of critical importance in the separation of the deuteron analysing powers for the $dp \to (pp)n$ reaction and so it necessary to have a reasonable understanding of its behaviour within a reliable simulation. As can be seen from Fig. 5.2, this has been successfully achieved.

5.1.3 Cross–section determination

Having corrected the number of events for acceptance and DAQ (deadtime) and other efficiencies, the cross sections found on the basis of the quasi-free $np \to d\pi^0$

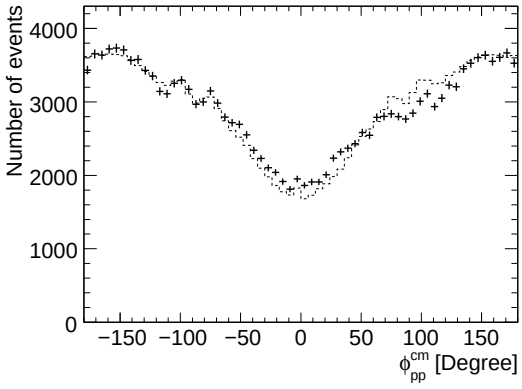

Figure 5.2: Distribution of $dp \rightarrow \{pp\}n$ events in the azimuthal angle ϕ obtained with an unpolarised beam for $E_{pp} < 3$ MeV (red) compared to a simulation of expected events (black).

luminosity were put in (E_{pp}, q) bins. The results obtained by summing these data over the interval in momentum transfer $0 < q < 100$ MeV/c are presented as a function of E_{pp} in Fig. 5.3.

The impulse approximation predictions, also shown in Fig. 5.3, describe these data reasonably well even in absolute magnitude, although the model seems to be be pushed to slightly higher values of E_{pp} than the data. It is important to note that, even for excitation energies as low as 3 MeV, there are significant contributions from higher partial waves. These arise preferentially for this reaction because even a small momentum kick to the neutron when it undergoes a charge exchange can induce higher partial waves because of the large deuteron radius.

The variation of the cross section with momentum transfer can be found in Fig. 5.3 for $0 < E_{pp} < 3$ MeV. The impulse approximation of section 1.2 also describes well the dependence on this variable out to $q = 140$ MeV/c. Once again it should be noted that no adjustment has been made to the model or the experimental data; the luminosity was evaluated independently using the quasi-free $np \rightarrow d\pi^0$ reaction.

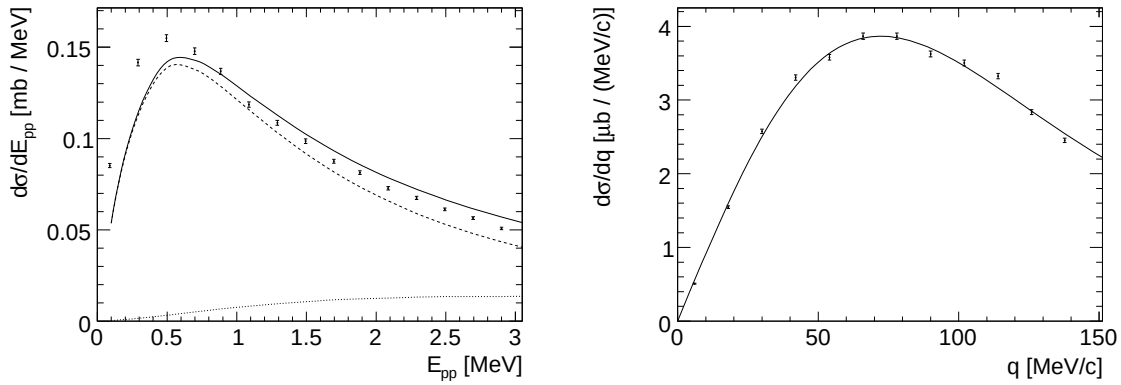

Figure 5.3: Left: Differential cross section for unpolarised $dp \to \{pp\}n$ integrated over momentum transfer $q < 100$ MeV/c as a function of the excitation energy E_{pp}. Only statistical errors are shown. The impulse approximation predictions are shown separately for the $^1S_0$ (dashed) and higher waves (dot-dashed) as well as their sum (solid curve). **Right:** Unpolarised differential cross section for the $dp \to (pp)n$ reaction for $E_{pp} < 3$ MeV compared with the impulse approximation predictions. Only statistical errors are shown. There is in addition a global systematic uncertainty of about 6%.

5.2 Deuteron beam polarisation

We already showed that the charge–exchange breakup reaction should show significant polarisation effects. If analysing powers are measured it can be very nice tool for the beam polarimetry because of its high cross–section. The measurement of a variety of nuclear reactions in ANKE showed that there was negligible loss of beam polarisation when the deuterons were subsequently brought up to the experimental energy of $T_d = 1170$ MeV (Ch. 3.)

Although the EDDA systematic uncertainties are quite low, as can be seen from Table 5.1, only limited statistics were collected and these we alleviate by using the internal consistency of our deuteron charge–exchange data themselves. According to impulse approximation predictions [8, 13], the deuteron vector analysing power for the $\overrightarrow{d}\,p \to (pp)n$ reaction should vanish for small excitation energies. Since the values of P_z can have no effect for $\theta_{pp} \approx 0$, this hypothesis can be tested by comparing the charge–exchange count rates, normalised on the BCT, for small and larger diproton angles. Any deviations from linearity could be ascribed to a it_{11} dependence since Table 5.1 shows that the eight states have widely different values of P_z. All the data presented in Fig. 5.4 (left panel) fit well to a straight line, which reinforces the belief that the charge exchange is, as expected, only sensitive to the

Mode	P_{zz}^{Ideal}	P_{zz}^{EDDA}	$P_{zz}^{\text{Stand.}}$
0	0	0	-0.006 ± 0.016
1	0	0.057 ± 0.051	0.040 ± 0.016
2	+1	0.594 ± 0.050	0.658 ± 0.032
3	–1	-0.634 ± 0.051	-0.575 ± 0.032
4	$-\frac{1}{2}$	-0.282 ± 0.064	-0.359 ± 0.024
5	+1	0.537 ± 0.064	0.594 ± 0.030
6	+1	0.545 ± 0.061	0.440 ± 0.024
7	$-\frac{1}{2}$	-0.404 ± 0.065	-0.355 ± 0.024

Table 5.1: The configurations of the polarised deuteron ion source, showing the ideal values of the tensor polarisations and their measurement using the EDDA polarimeter at a beam energy of $T_d = 270$ MeV [60]. The standardised values of P_{zz} obtained on the basis of all the deuteron charge–exchange data are given in the final column. However, it should be noted that mode-0 was indeed completely unpolarised and the statistical error quoted here is merely to show that the charge–exchange data were completely consistent with that.

value of P_{zz}.

In Fig. 5.4 (right panel) the totality of the charge–exchange data is compared to the values of P_{zz} measured with the EDDA polarimeter. The scatter is larger due to the EDDA statistical errors but a linear fit is a good representation of the data. We then replace the EDDA values of P_{zz} for each of the individual states by those corresponding to the linear regression shown in Fig. 5.4 (right panel) and these modified values are given in Table 5.1. This procedure retains the average dependence on the EDDA polarisations while reducing the statistical fluctuations inherent therein.

5.3 Analysing power measurement

Having identified the $np \to d\pi^0$ events, these were binned in intervals of di-proton excitation energy E_{pp} and three–momentum transfer $q = \sqrt{-t}$, and corrected for luminosity with the help of the beam current information in order to evaluate the analysing powers. In the right–handed coordinate system of the reaction frame, the beam defines the z–direction while the stable spin axis of the beam points along the y–direction, which is perpendicular to the COSY orbit. The differential cross

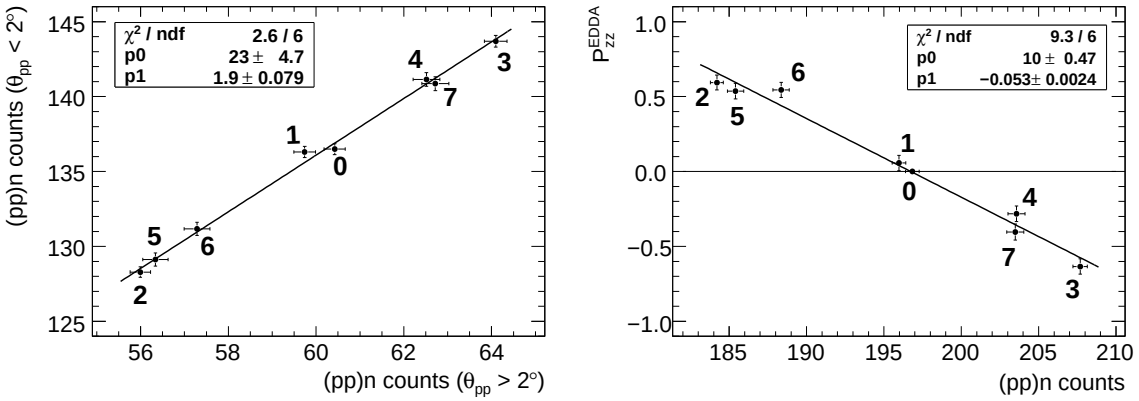

Figure 5.4: Normalised counts $\times 10^{-3}$ for the $dp \to (pp)n$ reaction for the eight different source modes of Table 5.1, (left panel) for events where the diproton laboratory angle is less than 2° compared to events where the angle is greater than 2°, and (right panel) compared to the EDDA measurements of the beam tensor polarisation [60]. Also shown are straight line fits to the data.

section for a polarised $\overrightarrow{d}\,p \to (pp)n$ reaction then becomes

$$\frac{\mathrm{d}\sigma}{\mathrm{d}t}(q,\phi)\Big/\left(\frac{\mathrm{d}\sigma}{\mathrm{d}t}(q)\right)_0 = 1 + \sqrt{3}P_z it_{11}(\theta)\cos\phi - \frac{1}{2\sqrt{2}}P_{zz}t_{20}(\theta) - \frac{\sqrt{3}}{2}P_{zz}t_{22}(\theta)\cos(2\phi)\,, \tag{5.2}$$

where the 0 subscript refers to the unpolarised cross section. Here θ and ϕ are, respectively, the polar and azimuthal angles of the diproton, with the latter being measured from the COSY machine plane. it_{11} (t_{20}, t_{22}) are vector (tensor) analysing powers of the $\overrightarrow{d}\,p \to (pp)n$ reaction [40].

For each of the seven intervals in q (about 20 MeV/c width), the yield was sorted in ten bins in $\cos 2\phi$. Although it is clear from Fig. 5.2 that the acceptance in terms of the azimuthal angle ϕ is well reproduced by the simulation, we have used states–0 and –1, where there is zero tensor polarisation, to provide the best estimate of the denominator in Eq. (5.2). By doing this we are using the fact that the geometric acceptances should be universal, *i.e.*, independent of the polarisation state of the source. An example of the linear fit is shown in Fig. 5.5 for polarisation state–5.

The analysing powers of the $\overrightarrow{d}\,p \to (pp)n$ reaction were subsequently evaluated by fitting with Eq.(5.2) and using the beam polarisations of states–2 to –7 quoted in Table 5.1. An estimate of the statistical errors inherent in this procedure could

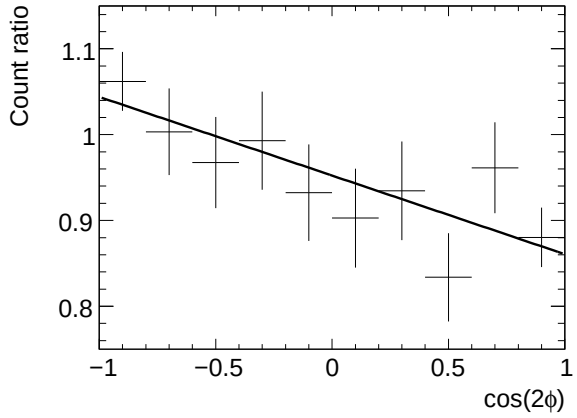

Figure 5.5: Azimuthal angular dependence of the ratio of the normalised $dp \to (pp)n$ count rates for the source mode–5 to the average of modes–0 and –1, which have no tensor polarisation. Here the data are shown for the bin $40 < q < 60$ MeV/c and $E_{pp} < 1$ MeV. The linear fit in $\cos 2\phi$ allows the analysing power to be extracted by fitting the data to the right hand side of Eq. (5.2).

be obtained by studying the scatter of the results for these six polarisation states of the source. In impulse approximation the vector analysing power is predicted to vanish for small E_{pp} [8]. A similar procedure in terms of $\cos\phi$ allowed bounds to be obtained on the vector analysing power but, as expected from both theory and the linearity of Fig. 5.4 (left panel), all the data are consistent with it_{11} vanishing within error bars. The averages over the whole q range are $< it_{11} >= -0.001 \pm 0.004$ for $E_{pp} < 1$ MeV and -0.004 ± 0.004 for $1 < E_{pp} < 3$ MeV.

Due to the limited ANKE angular coverage, the acceptance gets steadily poorer as q and E_{pp} increase, so that values of analysing powers could only be determined for $q < 130\,\mathrm{MeV/c}$. Our experimental values of the two tensor analysing powers are shown in Fig. 5.6 for the two ranges in E_{pp} as a function of the momentum transfer. The signals both fall when E_{pp} rises due to the influence of higher partial waves. It is known that, when $\vec{q}$ and the pp relative momentum $\vec{k}$ are perpendicular, odd partial waves cannot be excited and the pp system must be in a spin–singlet state [8]. As a consequence, less triplet dilution of the analysing powers is expected for small $\cos\theta_{qk}$. To show this, we have divided the data shown in Fig. 5.6 into the two regions where $|\cos\theta_{qk}| \lesseqgtr 0.5$ and imposed the same cuts on the theoretical description. All the features of both t_{20} and t_{22} are then reproduced, including the variation with q, E_{pp}, and $\cos\theta_{qk}$. It seems therefore that the model is as valid here as at lower energies [11] and that, as predicted in Ref. [8], multiple scatterings do

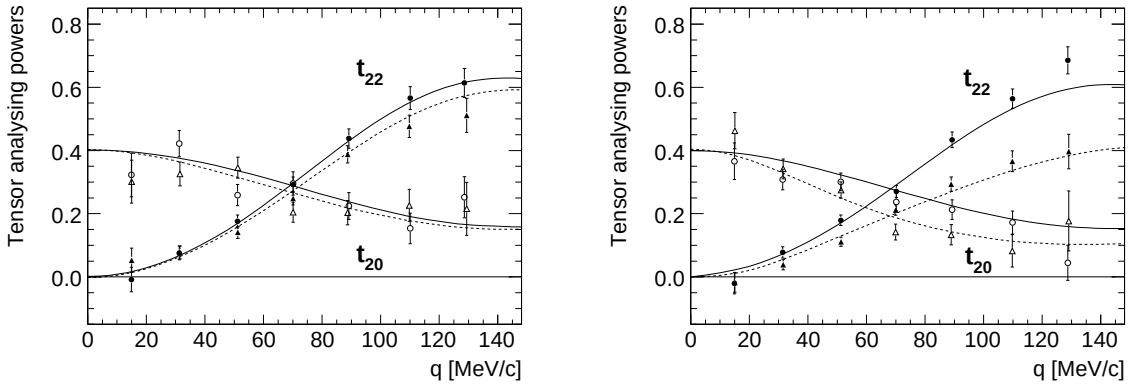

Figure 5.6: Spherical tensor analysing powers t_{20} and t_{22} for the CE reaction at $T_d = 1170$ MeV for (a) $0.1 < E_{pp} < 1.0$ MeV and (b)$1.0 < E_{pp} < 3.0$ MeV. The circles correspond to data where $|\cos\theta_{qk}| < 0.5$ while the stars denote the results for $|\cos\theta_{qk}| > 0.5$. The solid and dashed curves are the impulse approximation predictions for the same angular selections, respectively.

not distort the analysing powers significantly.

The rapid rise of t_{22} with q is mainly a result of the fall in the $\delta(q)$ amplitude which, in a simple absorbed one–pion–exchange model, should vanish for $q \approx m_\pi c$. The behaviour can therefore be understood semi–quantitatively on the basis of Eq. (6.1). The much smoother variation of t_{20} is also expected, with a gentle decline from the forward value, once again being mainly driven by the fall in the $\delta(q)$ amplitude. All these features are well reproduced by the impulse approximation model [13] using reliable np amplitudes [3].

Although all the experimental data agree with the impulse approximation model one could, of course, invert the question. How well could one determine the amplitudes if there were no information available from the np phase shifts? Although the data reported here were obtained over only a two–day run, these are already sufficient to determine quite well the ratio of the $|\varepsilon(0)|/|\beta(0)|$ in the forward direction. Since little dilution of the t_{20} signal is expected at $q = 0$, all the data for $E_{pp} < 3$ MeV were fitted to a quadratic in q^2 for $q \leq 100$ MeV/c. The value obtained at the origin gives $t_{20} = 0.37 \pm 0.02$, where the error is purely statistical. The uncertainty introduced by the beam polarisation would, however, contribute less than ± 0.01 to this. Since there is little or no dilution of the analysing power by the P-waves at $q = 0$, this result translates into an amplitude ratio of

$$|\varepsilon(0)|/|\beta(0)| = 0.61 \pm 0.03\,. \tag{5.3}$$

The precision here is, of course, better than that which is achieved for the absolute value of the forward amplitudes discussed in chapter 1, where the overall normalisation and other effects introduces another 5% uncertainty.

5.4 Summary and conclusions

In this study we have shown that the measurement of the differential cross section and two deuteron tensor analysing powers of the $\overrightarrow{d}\,p \to (pp)n$ reaction at 585 MeV per nucleon allows one to deduce values of the magnitudes the amplitudes $|\beta(q)|^2 + |\gamma(q)|^2$, $|\delta(q)|^2$, and $|\varepsilon(q)|^2$. The results achieved agree very well with modern phase shift analyses [3]. There is no obvious reason why this success should not be repeated at higher energies where the neutron–proton database has far more ambiguities.

In addition to extending the ANKE measurements to the maximum COSY energy of 1.15 GeV per nucleon, experiments will be undertaken with polarised beam and target. The values of the two vector spin–correlation parameters depend upon the interferences of ε with the β and δ amplitudes [61]. Furthermore, the use of inverse kinematics with a polarised proton incident on a polarised deuterium gas cell will allow the study to be continued up to 2.9 GeV per nucleon [12].

On the other hand the low excitation energy charge exchange on the deuteron gives no direct information on the spin–independent amplitude α, whose magnitude can only be estimated by comparing the deuteron data with the free $np \to pn$ differential cross section. As seen from Eq. (1.11), at least in the forward direction the value of $|\alpha(0)|^2$ can be determined with respect to the other amplitudes by measuring the ratio of the charge exchange on the deuteron and proton [7].

At $q = 0$ there is potential redundancy between the measurement of the $\overrightarrow{d}\,p \to (pp)n$ and $np \to pn$ cross sections, though the normalisation is much easier to achieve with a beam of charged particles. Using this information in association with data on total cross section differences, it seems likely that a clear picture of the neutron–proton charge–exchange amplitudes in the forward direction is likely to emerge [6].

Chapter 6

Outlook

Our study of the $\vec{d}p \rightarrow (pp)n$ deuteron charge–exchange reaction presented in this thesis has shown that we can successfully investigate reactions with a polarised deuteron beam. In particular, we have proved that we can calibrate the vector and tensor polarisations of such a beam. Furthermore the results presented in this work show that we can contribute to the np-database with a very valuable data.

The Spin Programme at ANKE [12] includes the study of the $\overrightarrow{d}\,p \rightarrow (pp)n$ reaction up to maximum avaliable energy (2.23 GeV) at COSY. Since there is no possibility to do the deuteron polarimetry at higher energies, we propose to use the polarisation export technique [62]. The other major goal of the Spin Programme [12] is the double polarised study of the $\vec{d}\vec{p} \rightarrow (pp)n$ reaction to extract the spin correlation coefficients. For this purpose it is crucial to handle simultaneously the polarised beam and polarised target (cell–type), and establish the polarisation standards for double–polarised nuclear reactions at COSY energies. The experimental details of the polarisation export technique and the status towards the double–polarised measurements at ANKE are described in this chapter.

6.1 Polarisation export

Usually the absolute value of the beam polarisation is determined from the scattering asymmetry in a suitable nuclear reaction with known analysing powers. Polarisation calibration standards described in the thesis (Sec. 3) are few and exist only at discrete energies. It is therefore of great practical interest of the spin programme to

be able extend their application to arbitrary energies where standards are not yet available. Now, if care is taken to avoid depolarising resonances in the machine, the beam polarisation should in general be conserved during the process of ramping the beam energy up or down [62]. There are no any deuteron depolarisation resonances in COSY energy region and this should make things easier. In order to verify the polarisation export technique with a circulating deuteron beam at COSY, the scheme illustrated diagrammatically in Fig. 6.1 was implemented.

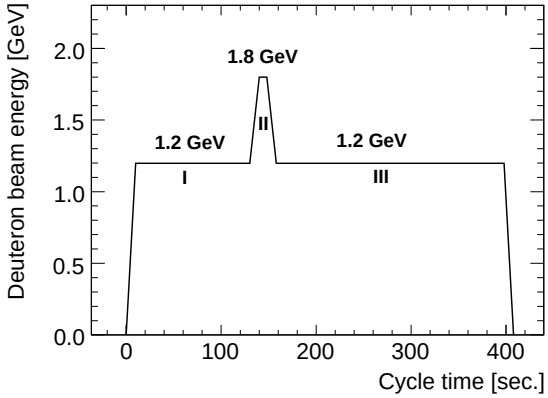

Figure 6.1: The schematic picture of the three different flat-top regions used in a single cycle. The identity of the deuteron polarisation in regions I and III means that 1.2 GeV polarisation could be exported to 1.8 GeV.

Using the $dp-$elastic reaction, which is sensitive to both vector and tensor polarisations of the beam, we have measured the polarisation for the regions I and III. The results are presented in the table 6.1 in terms of the non-normalised parameters β where the analysing power of the reaction has not been observed. Given that, within the small error bars, $\beta^{I}_{y/yy} = \beta^{III}_{y/yy}$ no depolarisation has been observed.

Flat top	β_y	β_{yy}
I	-0.213 ± 0.005	0.057 ± 0.003
III	-0.216 ± 0.006	0.059 ± 0.003

Table 6.1: The table shows the results of the asymmetry measurements for the I and III regions (Fig.6.1). β_y and β_{yy} represents the asymmetry for the vector and tensor component of the polarisation and respectively

The polarisation export technique appears to be a useful tool for the polarisation

experiments at any available energy at COSY. The data on 1.6 GeV, 1.8 GeV and 2.23 GeV energy were already taken and the data analysis is in progress.

6.2 Spin–correlation predictions

At low excitation energies E_{pp} of the final pp system, the spin observables in $\vec{d}\vec{p} \to (pp)n$ reaction are directly related to the spin–dependent parts of the neutron–proton charge–exchange amplitudes β, γ, δ and ε.

Impulse approximation applied to $dp \to (pp)_{^1S_0}n$ leads to the following predictions for the differential cross section, deuteron analysing powers, and spin–spin correlation parameters in hte pure $^1S_0$ limit:

$$\begin{aligned}
\frac{d^4\sigma}{dtd^3k} &= \tfrac{1}{3} I \left\{ S^-(k, \frac{1}{2}q) \right\}^2 , \\
I\, A_y^d &= 0\,, \; I\, A_y^p = -2\Im(\beta^*\gamma)\,, \\
I\, A_{xx} &= |\beta|^2 + |\gamma|^2 + |\varepsilon|^2 - 2|\delta|^2 R^2\,, \\
I\, A_{yy} &= |\delta|^2 R^2 + |\varepsilon|^2 - 2|\beta|^2 - 2|\gamma|^2\,, \\
I\, C_{y,y} &= -2\Re(\varepsilon^*\delta)R, \; I\, C_{x,x} = -2\Re(\varepsilon^*\beta).
\end{aligned}$$

Within this approximation, a measurement of the differential cross section, and deuteron analysing powers A_{xx}, and A_{yy} allowed us the extraction of $|\beta|^2 + |\gamma|^2$, $|\delta|^2$, and $|\varepsilon|^2$ over a range of values of q (three–momentum transfer) near the forward direction. The results of this study has been presented in previous chapters.

As a next step the measurement of the deuteron–proton spin correlation will allow us to determine the relative phases of these amplitudes and not just their overall magnitudes. Numerical predictions have been made for the transverse spin–correlation coefficients and the results are shown in Fig 6.2.

The predicted $C_{x,x}$ and $C_{y,y}$ are both expected to be very large and show considerable structure over the ANKE measurement range. We are quite fortunate to have found such a large (predicted) signal with such an interesting behaviour. Measurements of this observables are the primary aim of the experiment planned at COSY for the beginning of 2009.

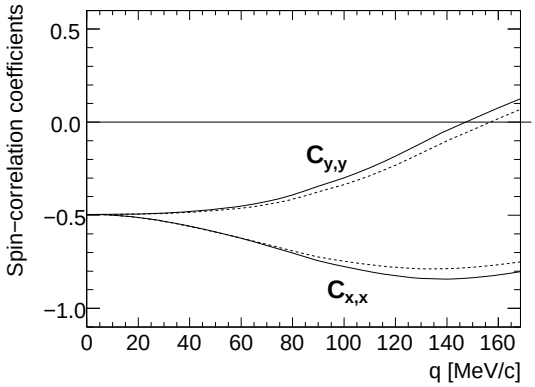

Figure 6.2: Predicted values of the spin–correlation coefficients in the CE reaction at 585 MeV/nucleon for cuts in excitation energy of $E_{pp} < 1$ MeV (solid line) and $E_{pp} < 3$ MeV (dashed line).

6.3 Results from first double–polarised measurements

Since summer 2005, the ANKE spectrometer is equipped with a Polarised Internal Target (PIT). During one week of a commissioning experiment in January 2007 allocated for the measurement of the Charge–Exchange break-up of polarised deuterons on a polarised hydrogen target $\overrightarrow{d}\,\overrightarrow{p} \to (pp)n$, the following results have been achieved:

- For the first time, studies with the COSY polarised deuteron beam were performed using a storage cell (25 μm aluminum foil, with the inner surface covered by Teflon, of 20×15 mm^2 cross section and 390 mm length). For this purpose the machine group furnished a polarised deuteron beam, electron cooled, stacked at injection and accelerated to T_d=1.2 GeV;

- To improve the COSY beam intensity, a longer stacking injection was implemented. In double–polarised measurements we worked with a cycle of 45(50) minutes duration: 15(20) minutes for stacking (90(120) stacks separated by 10 s for cooling) and 30 minutes for the flat top. Under these conditions 7×10^9 polarised deuterons were accelerated to the flat–top energy of 1.2 GeV;

- It has been shown that the procedure of scraping the accelerated beam before the data–taking minimised the background events coming from the interactions of the beam halo particles with the cell wall. Even without using stochastic cooling (this is not possible at COSY at the beam energy of $T_d = 1.2$ GeV),

the achieved beam quality generally allowed the deuterons to pass through the cell without touching the walls;

- The expected density for the polarised hydrogen ($\vec{\mathrm{H}}$ gas) storage cell target of $d_t = 1.34 \times 10^{13}\,\mathrm{cm}^{-2}$ was achieved. This value, together with the beam intensity of 7×10^9 stored polarised deuterons, led to a luminosity of $L \simeq 1.0 \times 10^{29}\,\mathrm{s}^{-1}\mathrm{cm}^{-2}$;

- The clean identification of events for the $\vec{d}\vec{p}$–induced reactions when using a long cell target has been demonstrated. This was done on the basis of experimental information obtained from the $\vec{\mathrm{H}}$ gas target and on the known shape of the background from the cell walls, which is imitated through the use of N_2 gas in the cell. The exact shape of the background under the missing–mass peak from the cell–wall events has been determined under real experimental conditions and was under control during on-line measurements;

- Using the missing–mass technique for the measured single–and double–track events in ANKE, it has been shown that very clean identification of the following reactions is possible: $\vec{d}\vec{p} \to dp_{sp}\pi^0$ (both branches of quasi–free $\vec{n}\vec{p} \to d\pi^0$), $\vec{d}\vec{p} \to (pp)n$, $\vec{d}\vec{p} \to {}^3\mathrm{He}\,\pi^0$, and $\vec{d}\vec{p} \to dp$. The last channel was identified unambiguously with very little background by using the silicon detectors, placed closed to the storage cell in vacuum target chamber, in coincidence with the forward detector system;

- In parallel to the data–taking, the ABS source has been tuned with Lamb–shift Polarimeter (LSP) measurements (see Fig. 6.3). The goal was to determine the target polarisation (Q_y) from the quasi–free $n\vec{p} \to d\pi^0$ reaction (see Fig. 6.3). The achieved value of average target polarisation of $\langle Q_y \rangle = 0.75 \pm 0.06$, is much higher then it was in the the first measurements in 2006. Thus, the target polarisation has been maximised and the equality of positive and negative polarisations has been verified on the level of a couple of percent by using on–line measurements from the LSP, repeated every 24 hours;

- We have extracted the value of the deuteron beam vector polarisation P_z from the quasi–free $\vec{n}p \to d\pi^0$ reaction using the angular dependence of the analysing power of the $\vec{p}p \to d\pi^+$ reaction, which was also used to determine the target polarisation. The result, $\langle P_z^{ANKE} \rangle = 0.60 \pm 0.10$, is compatible

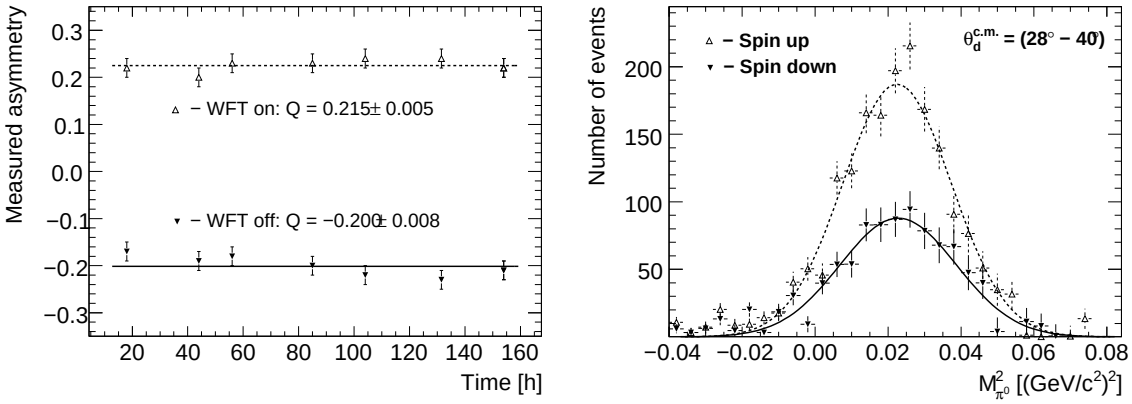

Figure 6.3: Left: On–line measurements of the Lyman–α peak asymmetry from the LSP when the weak field transition unit (WFT) was switched **on** ('spin-up') and **off** ('spin-down'). **Right:** Angular dependence of the missing–mass squared distribution for the reaction $\boldsymbol{d\vec{p} \rightarrow dp_{sp}X}$ measured with the storage cell and 1.2 GeV deuteron beam. Red and black histograms stand, respectively, for data with target polarisation 'spin-up' and 'spin-down', after background subtraction using N_2 data.

with the value of $\langle P_z^{LEP} \rangle = 0.660 \pm 0.003$, obtained from the Low Energy Polarimetry (LEP) measurements.

Given the above successes in the first handling of the double–polarised data, we can conclude that ANKE–COSY is ready to embark on the experimental programme which includes the double–polarisation measurements.

Acknowledgments

In this small but very important chapter I would like to express my gratitude to those who supported me during this very exciting time of being a PhD student.

My greatest debt is to Prof. Dr. H. Ströher for providing the opportunity to work in his group in Forschungszentrum Jülich. His careful reading of my original manuscript and his detailed, perceptive comments contributed to the shape and clarity of the finished thesis.

I would like to thank Prof. Dr. M. Nioradze with whom I began to work on this interesting topic for the trust and support. I am grateful to Dr. A. Kacharava for being my supervisors in Jülich and provided ceaseless help in both structuring and writing this thesis. I am thankful to our group leader Dr. F. Rathmann for his comments, and willingness to discuss any questions or ideas that I have had.

I would like to thank Dr. S. Dymov for many conversations which provided insight about the data analysis and simulation – especially in the beginning when everything was very new and seemed very difficult. Dr. M. Hartmann, Dr. A. Mussgiller and Dr. V. Hejny also provided assistance and shared their experience in software development, which was very important for the data analysis. Apart that the programming was always a very interesting subject for me.

It is difficult to overstate my debt to Prof. Dr. C. Wilkin, whose thoughtful advice often served to give me a sense of direction during my PhD study. I would like to express my gratitude for his great efforts to explain things clearly and simply, and without whom I would have been lost a long time ago.

I would like to express my gratitude to my Georgian colleagues Dr. I. Keshelashvili, Dr. G. Macharashvili and many others for there support and assistance.

This thesis would not have been possible without the assistance of members of the ANKE collaboration, COSY crew, and IKP staff, who are really the great colleagues and created a very good atmosphere to work in.

I also want to thank my friends who were always very supportive and never let me feel alone. Many of them don't really understand the physics but were always curious about my work and it always was a lot of fun.

And finally, I want say many thanks to my family for their patience, understanding and invaluable support while being so far from home. For their love and care for whole my life and simply for being the best family on the Planet to whom I dedicate this work.

Appendix A

Principles of polarisation

In quantum mechanics all spin angular momentum operators S_i satisfy the equation:

$$S_i S_j - S_j S_i = \epsilon_{ijk} S_k \tag{A.1}$$

These spin operators are hermitian and their trace is 0. We have three components in a Cartesian coordinate system S_x, S_y, and S_z which defines the vector $\vec{S}$. Their eigenvalues and eigenfunctions satisfy:

$$\vec{S}^2 \left|sm\right\rangle = s\left(s+1\right)\hbar \left|sm\right\rangle \tag{A.2}$$

$$S_z \left|sm\right\rangle = m\hbar \left|sm\right\rangle \;\; m = -s, -s+1, ..., +s \tag{A.3}$$

$\left|sm\right\rangle$ is the eigenfunction of $\vec{S}^2$ and one of its projection, conventionally chosen to be the z projection. It depends on two quantum numbers: spin quantum number s and magnetic quantum number m. The number of values of m is $(2s+1)$.

When $s = 1/2$, we then have two values $m = -1/2$ or $m = +1/2$. We can write the spin operator in terms of matrices with the Pauli definition:

$$\vec{S} = \tfrac{1}{2}\hbar\vec{\sigma} \tag{A.4}$$

where

$$\sigma_x = \begin{pmatrix} 0 & 1 \\ 1 & 0 \end{pmatrix} \quad \sigma_y = \begin{pmatrix} 0 & -i \\ i & 0 \end{pmatrix} \quad \sigma_z = \begin{pmatrix} 1 & 0 \\ 0 & -1 \end{pmatrix} \tag{A.5}$$

The set of these three Pauli matrices and unit matrix form a complete set of hermitian matrices for $s = 1/2$. Every hermitian operator in these space is linear

combination of these operators.

A.1 Spin 1/2

The above describes a single particle with $\langle S_z \rangle = \pm\frac{1}{2}\hbar$ and corresponding $\langle \sigma_z \rangle = \pm 1$. It is, however, impossible to describe things in such a way when there is ensemble of particles (for example a beam). To represent such ensemble in quantum mechanics, it is convenient to define the density matrix:

$$\rho = \sum_{i=1}^{n} p_i \left| sm_i \right\rangle \left\langle sm_i \right| \tag{A.6}$$

With:
$n \equiv$ number of the pure states (here $n = 2$);
$p_i \equiv$ probability of i state in the ensemble.

It helps to describe polarisation with three components p_i $(i = x, y, z)$ which are the expectation values of the Pauli operators $\langle \sigma_i \rangle$. We can write it in the short way:

$$p_i = \langle \sigma_i \rangle = \text{Trace}\left(\rho \sigma_i\right) \tag{A.7}$$

These are the components of a vector $\vec{p} = (p_x, p_y, p_z)$. The polarization $\vec{p}$ is the vector polarization of the ensemble of particles with spin 1/2. Here we should be carefully because in quantum mechanics only one component can be measured. Taking this to be the z-component:

$$p_z^* = \langle \sigma_z \rangle = \text{Trace}\left(\rho \sigma_z\right) = p_+ \left\langle + \right| \sigma_z \left| + \right\rangle + p_- \left\langle - \right| \sigma_z \left| - \right\rangle = p_+ - p_- \tag{A.8}$$

When $p_z^* = 0$, it means that $p_+ = p_-$ and the probabilities of $|1/2, +1/2\rangle$ and $|1/2, -1/2\rangle$ states are equal. The state with $m = +1/2$ is populated with the same number of particles N_+ as the $m = -1/2$ states N_-.

If $p_+ > p_-$, it means that there are more particles in state $|1/2, +1/2\rangle$, and $N_+ > N_-$. So we have polarization along the z axis:

$$p_z^* = p_+ - p_- = \frac{N_+}{N_{tot}} - \frac{N_-}{N_{tot}} = \frac{N_+ - N_-}{N_+ + N_-}, \tag{A.9}$$

from which we evidently get:

$$-1 \leq p_z^* \leq +1. \tag{A.10}$$

If all particles in the beam are in the state $m = 1/2$, then we get polarization of the beam $p_z^* = 1$, or if all particles are in the state $m = -1/2$, we have $p_z^* = -1$.

A.2 Spin 1

There are three possible eigenvalues of S_z with its eigenfunctions from Eq. (A.3). So, we have three pure state for the spin 1 particles:

$$|s = 1; m = 1\rangle \quad |s = 1; m = 0\rangle \quad |s = 1; m = -1\rangle \tag{A.11}$$

The spin operator $\vec{S}$ is therefore a 3×3-matrix and one can write them like the Pauli operators:

$$S_x = \frac{1}{\sqrt{2}} \begin{pmatrix} 0 & 1 & 0 \\ 1 & 0 & 1 \\ 0 & 1 & 0 \end{pmatrix} \quad S_y = \frac{i}{\sqrt{2}} \begin{pmatrix} 0 & -1 & 0 \\ 1 & 0 & -1 \\ 0 & 1 & 0 \end{pmatrix} \quad S_z = \begin{pmatrix} 1 & 0 & 0 \\ 0 & 0 & 0 \\ 0 & 0 & -1 \end{pmatrix} \tag{A.12}$$

These three operators together, with 3×3 unit matrix, comprise four hermitian operators, which are linear independent. It is however evident that nine are needed to 'span' the 3×3 space. Each spin operator has to have zero trace and each will be orthogonal to the unit matrix U which means that its expectation value will be zero for an unoriented ensemble. One can construct from the available matrices:

$$S_{ij} = \frac{3}{2}(S_i S_j + S_j S_i) - 2U\delta_{ij} \qquad (\text{with } i, j = x, y, z) \tag{A.13}$$

With this one obtains six matrices but, since $\text{Trace}(S) = 0$, we get only five linear independent matrices:

$$p_{ij} = \langle S_{ij} \rangle = \text{Trace}(\rho S_{ij}) \tag{A.14}$$

We can define p_{ij} in a same way to p_i:

$$p_{zz} = \langle S_{zz} \rangle = \text{Trace}(\rho S_{zz}) \tag{A.15}$$

It is possible to compose a 3×3 matrix from the different components of p_{ij}, which is a second rank tensor, and defines a tensor polarization of the beam. The definition of the vector polarization is the same Eq. (A.12), but we can write p^*_{zz} with the occupation number of three spin states:

$$p^*_{zz} = \langle S_{zz} \rangle = \mathrm{Trace}(\rho S_{zz}) = p_+ + p_- - 2p_0 \tag{A.16}$$

If all three states are occupied equally in the beam, $p_+ = p_- = p_0 = 1/3$, then we have an unpolarized beam with $p^*_{zz} = 0$ and $p^*_z = 0$. In general

$$p^*_{zz} = p_+ + p_- - 2p_0 = \frac{N_+ + N_- - 2N_0}{N_{tot}} \tag{A.17}$$

From this it follows that:

$$-2 \leq p^*_{zz} \leq 1 \tag{A.18}$$

For illustration see Fig. A.1. Knowing the tensor polarization gives us information

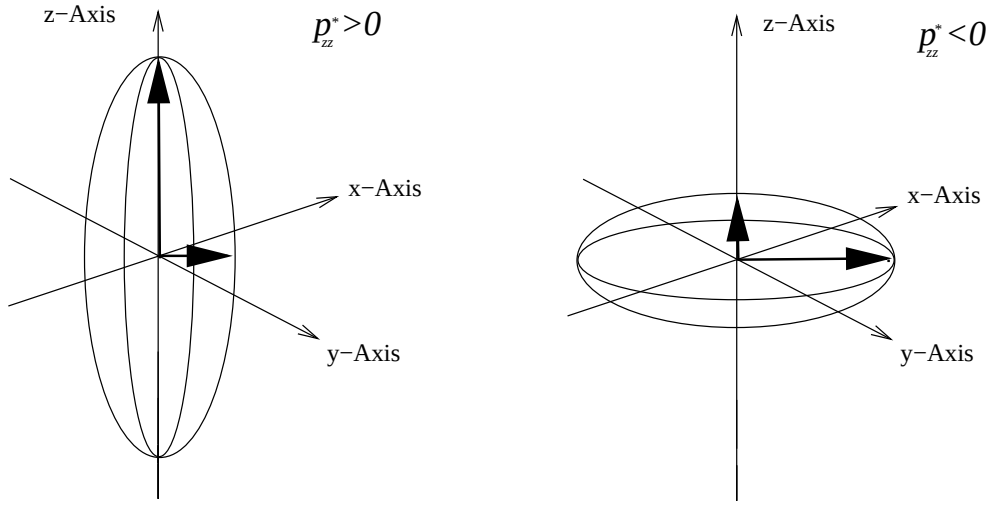

Figure A.1: Positive and negative tensor polarizations

about the relation between $N_+ + N_-$ and N_0. The vector polarization (relation between N_+ and N_-), together with intensity $N_{tot} = N_+ + N_- + N_0$, gives us all the information about the occupation of the states.

Appendix B

Observables in double–polarisation measurements

Ohlsen has discussed in detail the observables that can be accessed when a polarised spin-1 particle collides with polarised spin-$\frac{1}{2}$ target [40]. In a right–handed coordinate system, with z pointing along the beam direction, y being perpendicular to the reaction plane, and x lying therein, the differential cross section σ for a dp–induced reaction can be written:

$$\begin{aligned}\sigma/\sigma_0 = 1 \;&+\; Q_y A_y^p + \tfrac{3}{2} P_y A_y^d \\ &+\; \tfrac{2}{3} P_{xz} A_{xz}^d + \tfrac{1}{3}(P_{xx}A_{xx} + P_{yy}A_{yy} + P_{zz}A_{zz}) \\ &+\; \tfrac{3}{2}(P_x Q_x C_{x,x} + P_x Q_z C_{x,z} + P_y Q_y C_{y,y} + P_z Q_x C_{z,x} + P_z Q_z C_{z,z}) \\ &+\; \tfrac{1}{3}(P_{xx} Q_y C_{xx,y} + P_{yy} Q_y C_{yy,y} + P_{zz} Q_y C_{zz,y}) \\ &+\; \tfrac{2}{3}(P_{xy} Q_x C_{xy,x} + P_{xy} Q_z C_{xy,z} + P_{yz} Q_x C_{yz,x} + P_{yz} Q_z C_{yz,z}), \qquad \text{(B.1)}\end{aligned}$$

where the polarised deuteron beam is described by the components P_i and P_{ik}, and the polarised hydrogen target by the components Q_i with $i, k = x, y, z$; σ_0 is the unpolarised cross section. The single polarisation observables are the proton analysing power A_y^p and the deuteron vector and tensor analysing powers A_y^d and A_{ik} $(i, k = x, y, z)$. In addition there are the vector and tensor spin–correlation coefficients $C_{i,k}$ and $C_{ik,j}$.

In our set–up, both the target proton and incident deuteron are polarised perpendicularly to the plane of the COSY ring, with polarisation Q and (P_z, P_{zz}) respec-

tively. In general the reaction plane lies at an azimuthal angle ϕ with respect to the COSY plane, where ϕ is measured *clockwise* from the positive x-axis, looking along the beam direction. In this system the differential cross section becomes [40, 63]

$$\begin{aligned}\sigma/\sigma_0 &= 1 + Q\,A_y^p \cos\phi + \tfrac{3}{2} P_z A_y^d \cos\phi + \tfrac{1}{4} P_{zz}\left[(A_{yy} + A_{xx}) + (A_{yy} - A_{xx})\cos 2\phi\right] \\ &+ \tfrac{3}{4} P_z Q\left[(C_{y,y} + C_{x,x}) + (C_{y,y} - C_{x,x})\cos 2\phi\right] \\ &+ \tfrac{1}{4} P_{zz} Q\left[(\frac{1}{2}C_{xx,y} + \frac{1}{2}C_{yy,y} + C_{xy,x})\cos\phi + (\frac{1}{2}C_{xx,y} - \frac{1}{2}C_{yy,y} + C_{xy,x})\cos 3\phi\right].\end{aligned} \tag{B.2}$$

In the case of two spin-$\frac{1}{2}$ particles collision, for beam and target polarisations P and Q normal to the COSY plane, the azimuthal angular dependence is [40]:

$$\sigma/\sigma_0 = 1 + \left(A_y^P P + A_y^Q Q\right)\cos\phi + \tfrac{1}{2} PQ\left[(A_{y,y} + A_{x,x}) + (A_{y,y} - A_{x,x})\cos 2\phi\right]. \tag{B.3}$$

Here $A_{x,x}$ and $A_{y,y}$ are spin–correlation parameters and A_y^P and A_y^Q are analysing powers for polarised beam and target, respectively. Note that for cases such as pp elastic scattering or $pn \to d\pi^0$, where there is a unique isospin, one has $A_y^P = A_y^Q$.

Bibliography

[1] J. Bystricky et al., Nucl. Phys. A444 (1985) 597.

[2] M. Altmeier et al., Phys. Rev. Lett. 85 (2000) 1819.

[3] R.A. Arndt, W.J. Briscoe, R.L. Workman, and I.I. Strakovsky,Phys. Rev. C **62**, 034005 (2000); `http://gwdac.phys.gwu.edu`.

[4] M. Rentmeester, http://nn-online.org

[5] I. Pomeranchuk, Doklady Akad. Nauk **77** (1951) 249.

[6] F. Lehar, C. Wilkin, Eur. Phys. J. A **37**, 143 (2008).

[7] N.W. Dean, Phys. Rev. D **5** (1972) 1661; N.W. Dean, Phys. Rev. D **5** (1972) 2832.

[8] D.V. Bugg, C. Wilkin, Nucl. Phys. A **467**, 575 (1987).

[9] C. Ellegaard et al., Phys. Rev. Lett. **59** (1987) 974.

[10] C. Ellegaard et al., Phys. Lett. B **231** (1989) 365.

[11] S. Kox *et al.*, Nucl. Phys. A **556**, 621 (1993).

[12] A. Kacharava, F. Rathmann, and C. Wilkin for the ANKE Collaboration, COSY Proposal #152, *Spin Physics from COSY to FAIR*, arXiv:nucl-ex:0511028.

[13] J. Carbonell, M.B. Barbaro, C. Wilkin, Nucl. Phys. A **529**, 653 (1991).

[14] R. Maier, Nucl. Instr. Meth. **A 390** (1997) 1.

[15] D. Prasuhn *et al.*, Nucl. Instr. Meth. **A 441** (2000) 167.

[16] D. Prasuhn *et al.*, Cooling at COSY, Workshop on Beam Cooling and Related Topics, Bad Honnef 2001, FZ Jülich, Matter and Material, V. **13**, ISBN 3-89336-316-5.

[17] P.D. Eversheim *et al.*, The Polarized Ion–Source for COSY *Proc. Int. Symp. High Energy Spin Physics*, eds. C.W. De Jager, J.E. Oberski, and P.J. Mulders, Amsterdam, The Netherlands, 1996, p. 306 (World Scientific, Singapore, 1997).

[18] R. Weidmann *et al.*, Rev. Sci. Instr. **67**, 1357 (1996).

[19] O. Felden *et al.*, *Proc.* 9^{th} *Int. Workshop on Polarized Sources and Targets*, Nashville, 2001, eds. V.P. Derenchuk and B. von Przewoski, Nashville, USA, 2001, (World Scientific, Singapore, 2002) p. 200.

[20] M. Eggert *et al.*, Nucl. Instr. Meth. A **453**, 514 (2000).

[21] W. Haeberli, Ann. Rev. Nucl. Sci. **17**, 373 (1967).

[22] A. Lehrach *et al.*, AIP Conf. Proc. **675**, 153 (2003).

[23] S. Barsov et al., Nucl. Instr. Meth. A462 (2001) 364.

[24] A. Khoukaz *et al.*, Eur. Phys. J. **D 5** (1999) 275.

[25] F. Rathmann *et al.*, AIP Conf. Proc. **675**, 924 (2003).

[26] V. Kleber *et al.*, Phys. Rev. Lett. **91** (2003) 172304.

[27] S. Barsov *et al.*, COSY Proposal #114, 2002, spokesperson: R. Schleichert.

[28] M. Büscher *et al.*, COSY Proposal #94, 2000, spokesperson: A. Khoukaz.

[29] V. Komarov *et al.* COSY Proposal #20 (1999), Spokespersons: V. Komarov, F. Rathmann.

[30] A. Kacharava et al., 'The polarized charge-exchange reaction', COSY proposal # 125, Spokesperson: A. Kacharava, F. Rathmann (2003).

[31] G. Borchert *et al.*, IKP FZ–Jülich Annual Report 1997, Jül-3505, Jülich, 1998, p. 59.

[32] R. Schleichert *et al.*, IEEE Trans. Nucl. Sci. **50**, 301 (2003).

[33] I. Lehmann *et al.*, Nucl. Instr. Meth. A **530**, 275 (2004).

[34] S. Barsov *et al.*, Eur. Phys. J. A **21**, 521 (2004).

[35] S. Yaschenko *et al.*, Phys. Rev. Lett. **94**, 072304 (2005).

[36] D. Protić *et al.*, IEE Trans. Nucl. Sci. **52** 3194 (2005).

[37] S.N. Dymov *et al.*, Trigger electronics for the forward and backward hodoscopes of ANKE, JINR Dubna, Communication of JINR, **E10200219**, 2002.

[38] V.S. Morozov *et al.*, Phys. Rev. ST Accel. Beams **8**, 061001 (2005).

[39] J. Arvieux *et al.*, Nucl. Instr. Meth. A **273**, 48 (1988).

[40] G.G. Ohlsen, Rep. Prog. Phys. **35**, 717 (1972).

[41] P.D. Eversheim, *Proc. of the Workshop on Polarized Ion Sources and Polarized Gas Targets*, eds. L.W. Anderson and W. Haeberli, Madison, Wisconsin, USA, 1993, AIP Conf. Proc. **293**, 92 (1993). M. Eggert, PhD thesis, University of Cologne (1999).

[42] S. Kato *et al.*, Nucl. Instr. Meth. A **238**, 453 (1985).

[43] E.J. Stephenson, G. Noid, and C.J.G. Onderwater, *A Deuteron Polarimeter for an EDM Search*, Abstract: B12.00001, 2005 April APS Meeting, available from http://www.iucf.indiana.edu/ dedm/conferences/tampatalk.ppt

[44] In order to improve the polarimetry directly at the COSY ion source, a new polarimeter for proton and deuteron beams, based on the concept of the ANKE Lamb–shiftpolarimeter, is presently being installed.
R. Engels *et al.*, Rev. Sci. Instrum. **74**, 4607 (2003);
R. Engels *et al.*, Rev. Sci. Instrum. **76**, 053305 (2005).

[45] B. Lorentz *et al.*, *Proc.* 9^{th} *European Particle Accelerator Conference*, Lucerne, Switzerland, 2004, ISBN 92-9083-231-2, p.1246 (2005).

[46] K. Sekiguchi *et al.*, Phys. Rev. C **65**, 034003 (2002).

[47] B. Chiladze *et al.*, Part. Nucl., Lett. **4**, 95 (2002).

[48] S. Dymov *et al.*, Part. Nucl. Lett. **2**, 40 (2004).

[49] C. Kerboul *et al.*, Phys. Lett. B **181**, 28 (1986). C. Kerboul, PhD thesis, University of Strasbourg (1987); A. Boudard (private communication).

[50] A. Wrońska *et al.*, Eur. Phys. J. A. **26**, 421 (2005).

[51] M. Haji-Said *et al.*, Phys. Rev. C **36**, 2010 (1987).

[52] see *e.g.* C. Furget *et al.*, Nucl. Phys. A **655**, 495 (1999).

[53] Pluto WEB page:`http://www-hades.gsi.de/computing/pluto/html/PlutoIndex.html`.

[54] M. Lacombe *et al.*, Phys. Lett. **101B**, 139 (1981).

[55] R.A. Arndt, I.I. Strakovsky, R.L.Workman, D.V. Bugg, Phys. Rev. C **48**, 1926 (1993);
`http://gwdac.phys.gwu.edu/analysis/pd_analysis.html/`

[56] E.T. Boschitz *et al.*, Phys. Rev. C **6**, 457 (1972).

[57] N. Katayama *et al.*, Nucl. Phys. A438 **685** (1985).

[58] R.J. Glauber, in *Lectures in Theoretical Physics*, ed. W.E. Brittin (Interscience, N.Y. 1959) vol. 1, p. 315.

[59] V. Komarov *et al.*, Phys. Lett. B **553**, 179 (2003).

[60] B. Lorentz *et al.*, in *Proceedings of the 9th European Particle Accelerator Conference, Lucerne, Switzerland, 2004* (EPS-AG CERN, Geneva, 2005), p. 1246.

[61] M.B. Barbaro, C. Wilkin, J. Phys. G **15**, L69 (1989).

[62] R.E. Pollock *et al.*, Phys. Rev. Lett. **91**, 072304 (2005).

[63] B. v.Przewoski et al., Phys. Rev. C **74**, 064003 (2006).